Contrib Mineral Petrol (1999) 136: 193–212

Martin J. Streck · Anita L. Grunder

Enrichment of basalt and mixing of dacite in the rootzone of a large rhyolite chamber: inclusions and pumices from the Rattlesnake Tuff, Oregon

Received: 1 June 1998 / Accepted: 5 February 1999

Abstract A variety of cognate basalt to basaltic andesite inclusions and dacite pumices occur in the 7-Ma Rattlesnake Tuff of eastern Oregon. The tuff represents $\sim$280 km^3 of high-silica rhyolite magma zoned from highly differentiated rhyolite near the roof to less evolved rhyolite at deeper levels. The mafic inclusions provide a window into the processes acting beneath a large silicic chamber. Quenched basaltic andesite inclusions are substantially enriched in incompatible trace elements compared to regional primitive high-alumina olivine tholeiite (HAOT) lavas, but continuous chemical and mineralogical trends indicate a genetic relationship between them. Basaltic andesite evolved from primitive basalt mainly through protracted crystal fractionation and multiple cycles ($\geq$10) of mafic recharge, which enriched incompatible elements while maintaining a mafic bulk composition. The crystal fractionation history is partially preserved in the mineralogy of crystal-rich inclusions (olivine, plagioclase $\pm$ clinopyroxene) and the recharge history is supported by the presence of mafic inclusions containing olivines of Fo_{80}. Small amounts of assimilation ($\sim$2%) of high-silica rhyolite magma improves the calculated fit between observed and modeled enrichments in basaltic andesite and reduces the number of fractionation and recharge cycles needed. The composition of dacite pumices is consistent with mixing of equal proportions of basaltic andesite and least-evolved, high-silica rhyolite. In support of the mixing model, most dacite pumices have a bimodal mineral assemblage with crystals of rhyolitic and basaltic parentage. Equilibrium dacite phenocrysts are rare. Dacites are mainly the product of mingling of basaltic andesite and rhyolite before or during eruption and to a lesser extent of equilibration between the two. The Rattlesnake magma column illustrates the feedback between mafic and silicic magmas that drives differentiation in both. Low-density rhyolite traps basalts and induces extensive fractionation and recharge that causes incompatible element enrichment relative to the primitive input. The basaltic root zone, in turn, thermally maintains the rhyolitic magma chamber and promotes compositional zonation.

M.J. Streck[1] · A.L. Grunder
Department of Geosciences,
Oregon State University,
Corvallis, Or 97331, USA

Present address:
[1] Department of Geology
Portland State University,
Portland, OR 97207-0751, USA
Tel.: (503) 725-3379
Fax: (503) 725-3025
e-mail: streckm@pdx.edu

Editorial responsibility: T.L. Grove

Introduction

Mafic and silicic magmatism are intimately linked based on the common occurrence of quenched mafic inclusions and mafic enclaves in silicic plutons, tuffs, and lavas (Bacon 1986; Didier and Barbari 1991). In many instances, such inclusions are the only record of the mafic underpinnings that play an important role as *heat* source to drive melting and differentiation or as *material* source for fractionation, mixing, or diffusion. Particularly in voluminous tuffs or plutons, the record of mafic input is sparse or only indirectly accessible through petrochemical arguments. An important question is whether mafic inclusions are representative of mantle input to crustal magmatism. In many instances, mafic inclusions are basaltic andesites, rather than basalts, and substantial enrichments of incompatible trace elements suggest either anomalous mantle sources (e.g., Walter et al. 1987; Freundt and Schmincke 1995; Elburg 1996) or overprinting by extensive differentiation in the crust (Wiebe 1997).

We here examine the composition, mineralogy, and textures of basaltic inclusions and scarce dacite pumices in the rhyolitic Rattlesnake Tuff with a view toward evaluating the compositional and thermal interactions between basalt and rhyolite. We argue that the existence of a density trap, such as a rhyolite chamber, causes

protracted differentiation of underplating basalts that in turn thermally maintain continued differentiation within the rhyolite. The Rattlesnake Tuff is a particularly suitable case study because: (1) it represents a large volume of strongly zoned, high-silica rhyolite magma, (2) it contains a wide range of comagmatic mafic inclusions that are samples of the mafic root zone of the silicic chamber, and (3) it includes dacite pumices that yield insights into the chemical exchange between basalt and rhyolite.

Geologic setting of the Rattlesnake Tuff

The Rattlesnake Tuff is part of westward-younging, silicic volcanism of the High Lava Plains of southeastern Oregon that ranges from Late Miocene to recent. Silicic volcanism includes dozens of rhyolite dome complexes and some ignimbrites (Walker 1970, 1974; MacLeod et al. 1976; Walker and Nolf 1981; Greene 1973; MacLean 1994) (Fig. 1). Regional basaltic magmatism pre- and post-dates silicic volcanism and is characterized mainly by thin high-alumina olivine-tholeiite (HAOT) lava flows (e.g., Walker 1979; Hart et al. 1984; Streck and Grunder 1996) that share many characteristics with mid-ocean ridge basalts. Dacite, andesite, basaltic andesite and basaltic trachyandesite are minor, but ubiquitous, along the High Lava Plains as domes, lava flows, pyroclasts or cognate inclusions (e.g., Parker 1974; Linneman and Myers 1990; MacLean 1994; Johnson 1995; Streck and Grunder 1996).

The Rattlesnake Tuff

The Rattlesnake Tuff erupted at 7.05 Ma from the western Harney Basin (Fig. 1). The ignimbrite is a single cooling unit with an estimated magma volume of 280 km^3 and consists of 99% high-silica rhyolite as pumices and glass shards, < 1% dacite pumices and

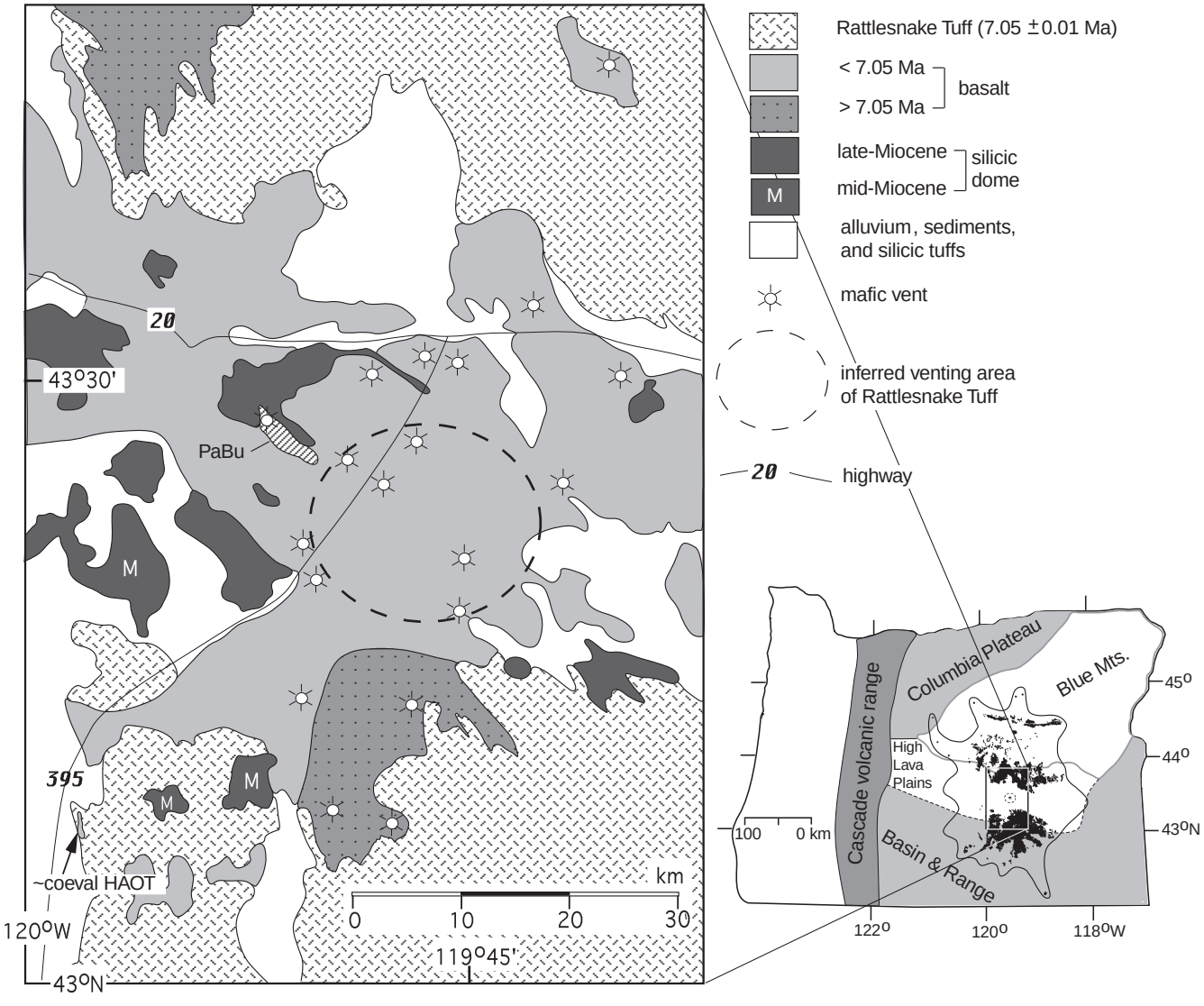

Fig. 1 Simplified geologic map of the western Harney Basin after Green et al. (1972). *PaBu* is Paiute Butte, a basaltic trachyandesite. *Arrow* points to locality of HAOT (high-alumina olivine tholeiite) basalt that are less than 300 K years younger to slightly older than Rattlesnake Tuff (see text and Table 1). Inset shows physiographic provinces of central and eastern Oregon and the outcrop pattern of the Rattlesnake Tuff (in *black*) with inferred pre-erosional distribution (*solid black line*)

$\ll$0.1% cognate basaltic inclusions (Streck 1994; Streck and Grunder 1995).

High-silica rhyolites

At least five distinct compositions of high-silica rhyolite occur as pumices and shards. They are distinguishable by color and chemical analysis and are related to one another by nonmodal crystal fractionation (Table 1, Fig. 2) (Streck and Grunder 1997). The most evolved ejecta are white, essentially aphyric, and are commonly concentrated in basal and distal parts of the tuff. Less differentiated shards and pumices are gray, contain ~1% phenocrysts (alkali feldspar, Fe-rich clinopyroxene, titanomagnetite ± quartz and fayalite) and are more abundant near the source and upsection (Streck and Grunder 1995). Both homogeneous and banded pumice clasts are common. The distribution of variably colored pumices and glass shards is interpreted to reflect sequential tapping of the most differentiated roof of a magma chamber to deeper less differentiated levels.

Dacites

Dacite pumices have distributions similar to the least evolved rhyolite. They are the principal bearers of mafic inclusions, indicating that mafic constituents resided beneath the rhyolite and were erupted late. Dacite occurs as vitric, black pumices (brown when oxidized) ranging from 2 to 30 cm in size. Uniformly black pumices are rare. Most dacite pumices are banded with variable proportions of high-silica rhyolite layers (Table 1, Fig. 2) and, less commonly, with basaltic streaks.

Basaltic inclusions

Basaltic material (inclusions and isolated phenocrysts) occurs dominantly in dacite or dacite-rhyolite banded pumices (Fig. 3). A few basaltic inclusions were recovered from the tuff matrix near the source area and they match inclusions found in pumices.

Basaltic material occurs as round or ellipsoidal bodies, as fine streaks with typical length-to-thickness ratios of 10 to 20, or as isolated single phenocrysts, with or without selvages of quenched basaltic groundmass (Fig. 3). The inclusions typically range from 3 cm to less than 1 mm long. All are interpreted to have been comagmatic based on (1) ellipsoidal shape or quenched crenulated margins indicating they were liquid, (2) quench textures of many plagioclase phenocrysts and of crystals in the glassy groundmass, and (3) compositional, textural, and mineralogical similarities among the basaltic inclusions indicating they are related (Fig. 3).

Among the sizeable inclusions ($>$3 mm long), three types are distinguished: *Crystal-poor inclusions*; *crystal-rich inclusions*, which contain abundant phenocrysts and (or) glomerocrysts; and *cumulus inclusions*, that commonly have cumulus texture and consist of ≥90% crystals.

Crystal-poor inclusions have the strongest mingling textures with host pumices. The quenched nature of the groundmass is clearly revealed only by reflected light microscopy or with help of backscatter electron images (Figs. 3a, b). Scarce phenocrysts are tabular plagioclase and olivine.

Crystal-rich inclusions all contain plagioclase and olivine, and some additionally contain clinopyroxene. Those with only olivine and plagioclase are commonly rounded and have fairly coarse quench textures in groundmass and of plagioclase phenocrysts, suggesting undercooling on the order of 100 to 200 °C (Figs. 3c, d) (cf., Lofgren 1980). Those that bear clinopyroxene phenocrysts have quench textures transitional between crystal-poor and other crystal-rich inclusions (Figs. 3g, h; Table 1). Strongly glomeroporphyritic inclusions are texturally transitional to cumulus inclusions with crystal content reaching 50% or more (Fig. 3f).

Cumulus inclusions consist either of plagioclase and clinopyroxene with minor FeTi oxides or of olivine and plagioclase, ± clinopyroxene. The former have cumulus texture and the latter granular texture, but we group them as cumulus inclusions. Clinopyroxene is poikilitic and scarce pockets of quenched interstitial groundmass indicate that the inclusions were not completely solidified when incorporated (Figs. 3k, l). The largest cumulus inclusion is 15 cm in diameter and is hosted in a dacite pumice.

Isolated basaltic phenocrysts (plagioclase, olivine, and augite) found in dacite, and rarely in rhyolite, can be readily identified because crystals are typically surrounded with a selvage of quenched basaltic groundmass or contain quenched mafic melt inclusions (Figs. 3e, i, j). Mafic selvages are commonly brick-red in handsample and black in thin section, contrasting well with brown dacite glass. The basaltic crystals are derived from disintegration or dispersion of mafic inclusion material (cf., Feeley and Dungan 1996).

Sample materials and analytical methods

Rhyolite and dacite pumices sampled from the Rattlesnake Tuff ranged in size from 5 to 40 cm. All pumices were glassy. LOI (loss on ignition) of rhyolites and most dacites was below 4 wt%. Five dacite pumices yielded LOI between 4 and 6 wt%. Major-element analyses were obtained from fused glass discs, with five times as much flux as rock powder, and selected trace elements concentrations were obtained from pressed powder pellets by X-ray fluorescence (XRF) at Stanford University. XRF data for inclusion samples 6exi1, 6exi2, 141A.i1, 2101B.i1, and 60Xi2 are from Washington State University. Seven crystal-rich inclusions, six crystal-poor inclusions, and all the components of one cumulus inclusion were analyzed for major and trace elements (Table 1). Other trace- and selected major-element concentrations were determined by instrumental neutron activation analysis (INAA) at the Radiation Center, Oregon State University. Analytical uncertainties are reported in Streck and Grunder (1997). Uncertainties previously not reported for major and minor elements by INAA for

Table 1 Chemical compositions of Rattlesnake Tuff whole-rock pumices and mafic inclusions, nearly coeval high-alumina olivine tholeiite, and compositional averages used in models. (Data normalized to 100% volatile free; *prn.total* total before normalization, *n.d.* not detected, *italicized numbers* are INAA values."*%-banded*" indicates hand-sample estimates of the proportion of high-silica rhyolite bands (*W* for white, *G* for gray) and basaltic bands (*M* for mafic); for example 7W4M indicates a dacite pumice with 7% white bands and 4% basaltic bands. Pumice data are from individual clasts)[a]

	High-silica rhyolites				Rhyolites (banded dacite pumices)			Dacites					
No.	RT-173H	RT-34E	RT-173B	RT-173A	RT-106A	RT-116B	RT-165B	RT-2A	RT-6D	RT-6E	RT-50A	RT-50B	RT-60B
HSR-group	A	B	D	E									
%-banded:					20W7M	30G2M	12G	3W	3W5M	1W1M	2W	5G	4G
XRF wt%													
SiO_2	77.67	77.18	76.59	75.70	69.54	70.19	70.23	63.18	68.48	64.80	61.92	64.53	65.83
TiO_2	0.11	0.12	0.14	0.16	0.66	0.66	0.58	1.26	0.80	1.11	1.41	1.14	1.05
Al_2O_3	11.96	11.77	11.97	12.47	12.90	12.78	12.87	13.40	12.67	12.94	13.80	13.38	13.18
Fe_2O_3	0.87	1.37	1.93	2.23	4.23	4.59	5.08	7.73	5.42	7.36	7.81	6.79	6.75
MnO	0.08	0.09	0.09	0.10	0.14	0.15	0.21	0.25	0.19	0.25	0.19	0.17	0.19
MgO	0.05	0.09	0.05	0.09	1.20	1.06	0.59	1.94	1.60	1.91	1.90	1.69	1.77
CaO	0.26	0.33	0.45	0.54	2.85	2.20	1.99	4.27	2.80	3.84	4.50	3.97	3.61
Na_2O	3.46	3.06	3.84	4.18	3.78	3.44	4.48	3.67	3.32	3.73	3.53	4.08	3.87
K_2O	5.53	5.95	4.92	4.59	4.31	4.63	3.69	3.47	4.33	3.38	4.18	3.69	3.22
P_2O_5	0.02	0.03	0.02	0.02	0.39	0.29	0.27	0.84	0.39	0.67	0.76	0.56	0.53
Prn.total	99.98	99.11	99.52	99.50	99.99	99.81	99.39	99.20	99.74	99.93	99.08	99.59	99.78
XRF ppm													
Rb	122	91	67	63	63	60	54	50	56	49	42	50	49
Ba	39	132	1230	1914	1260	1450	2220	1270	1440	1360	1240	1290	1450
Sr	2	4	12	26	108	83	99	162	104	153	185	168	140
Zr	175	308	433	460	372	421	638	470	433	497	375	374	428
Nb	39.4	32.0	27.2	25.4	25.3	25.2	26.1	23.5	25.2	24.5	20.8	22.2	23.4
Y	100	96	79	75	78	78	79	92	82	87	60	64	73
Pb	20	19	15	15	15	29	23	69	51	66	15	19	24.3
Zn	88	106	115	117	125	146	151	360	155	194	135	133	140
Ga	18	18	18	18	19	18	20	19	19	20	18	19	19
V	n.d.	6	2	17	103	46	20	79	55	68	90	83	76
Cu	1	2	4	3	17	12	7	15	17	17	23	20	19
Ni	14	10	10	9	19	14	9	18	18	18	21	13	16
Cr	n.d.	2.4	n.d.	3	15	10	1.3	20	15	16	46	23	22
INAA ppm													
FeO* wt%	0.78	1.22	1.69	2.09	3.70	4.01	4.40	6.91	4.74	6.43	6.91	5.80	5.97
Na_2O wt%	3.35	3.42	3.93	3.71	3.78	3.43	4.37	3.83	3.31	3.75	3.57	3.85	3.95
Cs	4.48	3.19	2.38	2.33	2.32	2.66	2.08	1.98	2.34	2.06	1.64	1.73	1.82
U	4.9	3.5	3.2	2.4	3.0	2.3	2.6	2.7	2.6	1.5	n.d.	2.2	1.7
Th	9.47	7.71	6.47	6.12	4.92	5.05	4.86	4.10	4.64	4.02	4.13	4.12	4.32
Hf	7.13	9.61	10.55	11.19	8.88	9.98	12.71	10.15	9.82	10.40	8.77	8.77	9.55
Ta	2.16	1.75	1.34	1.35	1.32	1.37	1.32	1.21	1.29	1.23	1.19	1.21	1.18
Sb	1.55	1.33	1.19	1.34	1.04	1.12	1.23	1.01	1.05	1.00	1.03	0.94	0.97
As	4.4	n.d.	3.9	4.5	n.d.	3.3	4.9	n.d.	4.3	4.1	n.d.	n.d.	3.9
Sc	3.93	3.69	3.76	4.83	13.06	13.28	16.73	25.63	16.10	24.10	23.96	19.78	21.00
Co	0.08	0.32	0.11	0.59	5.56	5.48	2.47	10.22	7.40	8.58	10.36	8.75	9.97

La	19.9	38.9	54.3	49.0	37.2	44.2	43.5	41.3	40.1	36.2	31.1	34.3	40.3
Ce	49	90	130	106	90	104	101	92	90	84	71	80	89
Nd	28	45	68	51	50	56	57	48	53	47	37	35	50
Sm	9.57	12.89	14.01	12.26	11.94	12.94	13.00	13.70	12.49	12.01	8.89	9.69	12.80
Eu	0.65	1.22	2.03	2.71	2.64	2.81	3.92	4.66	3.11	3.85	3.24	2.96	3.44
Tb	2.22	2.70	2.23	2.16	2.07	2.15	2.07	2.49	2.10	2.03	1.87	1.88	2.04
Yb	10.54	9.66	7.95	7.51	7.90	7.85	7.87	9.07	7.89	8.04	6.50	6.70	7.56
Lu	1.61	1.38	1.22	1.08	1.19	1.25	1.14	1.38	1.18	1.24	0.92	0.97	1.18

	Dacites					Nearly coeval HAOT			Averages & models		
No. %-banded	RT-60D 3G	RT-141A 5G	RT-165C 3W5G	RT-2101A 2G1M	RT-211A 2G	93.1ba	MiSi	HP33	Average dacite	Average xls-poor inclusion	Mafic endmember at 1:1 mix.
XRF wt%											
SiO_2	66.38	68.11	67.83	66.93	65.12	47.92	48.39	47.25	65.63	53.8(3)	56.0
TiO_2	0.90	0.87	0.85	0.90	1.15	0.98	1.05	0.77	1.03	2.05(11)	1.89
Al_2O_3	13.07	13.06	12.94	12.93	13.06	16.50	16.68	17.60	13.08	14.4(6)	13.8
Fe_2O_3	6.62	5.66	5.74	5.90	6.95	11.23	11.19	10.32	6.52	10.9(11)	10.8
MnO	0.23	0.18	0.20	0.19	0.21	0.20	0.18	0.21	0.20	0.34(27)	0.31
MgO	1.38	1.31	1.45	1.44	1.97	8.77	8.78	10.31	1.66	4.4(21)	3.23
CaO	3.22	2.79	2.98	2.90	3.71	11.62	10.86	11.32	3.51	7.3(16)	6.49
Na_2O	4.35	3.95	4.04	4.57	4.03	2.43	2.45	1.95	3.91	3.61(6)	4.22
K_2O	3.41	3.61	3.46	3.78	3.19	0.23	0.26	0.20	3.77	1.48(67)	1.82
P_2O_5	0.43	0.46	0.51	0.46	0.61	0.11	0.12	0.09	0.57	1.24(12)	1.11
Prn.total	99.05	99.99	99.71	99.50	99.96	100.33	99.77	99.73			
XRF ppm											
Rb	49	56	59	62	55	1.6	3	2	53.8	34(23)	43
Ba	1910	1380	1340	1260	1210	156	96	65	1382	1073(9)	841
Sr	143	108	124	118	146	383	205	197	143		262
Zr	621	411	455	438	419	51	64	47	440		413
Nb	25.8	25.3	26.2	26.5	24.4	1.2	2.3	2.1	24.6		23.2
Y	81	75	78	80	76	24	25	22	76.3		77
Pb	23	20	34	40	45	2.3	n.d.	1	33.8		55
Zn	154	136	153	162	162	73	70	55	157	368(41)	201
Ga	20	18	18	19	19	17	18	14	17		15
V	53	60	50	51	76	262	281	238	62		114
Cu	14	15	13	14	18	120	153	120	15		26
Ni	14	16	17	16	17	143	113	196	15		22
Cr	15	14	12	11	16	237	230	233	18	71(50)	33
INAA ppm											
FeO* wt%	5.84	4.95	5.06	5.19	6.29	10.1	9.61	8.17	5.75		
Na_2O wt%	4.30	3.78	4.01	4.66	3.79	2.30	2.22	1.88			
Cs	1.90	2.09	2.34	2.46	2.62	0.4	0.67	0.43	2.1	1.8(42)	1.83

Table 1 (Contd.)

	Dacites					Nearly coeval HAOT			Averages & models		
No.	RT-60D	RT-141A	RT-165C	RT-2101A	RT-211A	93.1ba	MiSi	HP33	Average	Average	Mafic
%-banded	3G	5G	3W5G	2G1M	2G				dacite	xls-poor inclusion	endmember at 1:1 mix.
U	2.9	2.2	2.5	2.8	1.8	n.d.	n.d.	n.d.	2.1		1.6
Th	4.23	4.67	4.92	4.93	4.50	0.17	0.29	0.44	4.41	2.42(22)	3.12
Hf	12.60	9.31	9.76	9.87	9.49	1.41	1.48	1.13	9.83	6.31(20)	8.6
Ta	1.33	1.30	1.42	1.36	1.32	0.08	0.10	0.07	1.27	0.95(14)	1.19
Sb	1.16	1.03	1.02	1.10	0.89	n.d.	n.d.	n.d.	1.00	0.89(16)	0.81
As	4.6	3.6	n.d.	4.6	3.1	n.d.	n.d.	n.d.			
Sc	22.00	16.94	18.02	18.80	22.60	47.5	42.5	40.4	20.5	36.5(8)	36.4
Co	7.24	7.60	6.89	6.94	9.76	49.7	44.4	43.4	8.39	20.4(13)	16.5
La	40.1	39.9	37.1	36.9	35.7	3.36	3.23	2.07	37.7	32.0(16)	24.4
Ce	92	96	87	80	86	8.0	7.8	5.7	87	74(16)	60
Nd	52	53	47	49	48	8.6	4.8	5.6	48	47(17)	41
Sm	13.08	12.28	12.05	12.59	12.10	2.42	2.41	1.76	12.0	12.4(14)	11.01
Eu	4.18	3.04	3.47	3.16	3.45	0.98	0.98	0.75	3.48	4.61(12)	4.32
Tb	2.13	2.12	2.13	2.08	2.07	0.62	0.59	0.45	2.08	2.31(13)	2.0
Yb	8.14	7.25	7.73	8.18	7.38	2.77	2.35	2.26	7.64	7.96(22)	7.48
Lu	1.21	1.08	1.18	1.24	1.10	0.40	0.37	0.34	1.15	1.19(24)	1.12

	Crystal[b]-rich inclusions							Cumulus inclusion			Phenocryst-poor inclusions					
Mineralogy	Ol & plag					Ol, cpx & plag		Cpx & plag								
No.	2A.i1	14D.i1	141A.i1	6exi1	6exi2	60Xi2	2101exi	60X.i1			6D.i1	6D.i2	106A.i1	106A.i4	116B.i1	2101B.i1
XRF-*INAA*	wt%							matrix	plag	cpx						
SiO_2			48.07	49.71	50.12	47.52	48.39									
TiO_2	*0.72*	*1.37*	1.43	2.23	1.70	1.86	2.43				*2.08*	*2.05*		*2.15*	*1.68*	*2.28*
Al_2O_3	*22.93*	*17.36*	18.27	17.57	18.98	17.15	15.96				*14.24*	*13.42*		*15.60*	*15.02*	*13.64*
Fe_2O_3*	*8.20*	*11.89*	12.17	11.15	10.01	12.64	13.25	*12.66*	*0.76*	*9.06*	*11.56*	*11.67*	*9.46*	*9.78*	*10.22*	*12.56*
MnO	*0.14*	*0.24*	0.18	0.13	0.14	0.22	0.25				*0.38*	*0.44*		*0.21*	*0.28*	*0.39*
MgO	*3.67*	*10.06*	6.05	3.84	3.49	6.40	4.95				*5.03*	*5.66*		*3.87*	*3.33*	*4.12*
CaO	*10.87*	*9.40*	9.94	10.36	11.10	9.75	9.55				*8.59*	*7.55*		*8.09*	*5.83*	*6.26*
Na_2O	*2.87*	*2.70*	2.91	3.54	3.39	2.90	3.09	*3.34*	*3.65*	*0.45*	*3.68*	*3.79*	*3.70*	*3.74*	*3.20*	*3.57*
K_2O	*0.4*	*0.3*	0.47	0.59	0.44	0.59	0.85				*0.73*	*0.78*		*1.91*	*2.76*	*2.67*
P_2O_5,*EMP*			0.51	0.87	0.62	0.99	1.29				*1.47(4)*	*1.09(8)*		*1.22(6)*	*1.14(6)*	*1.27(12)*
Prn.total	*49.80*	*53.32*	98.1	98.9	99.06	98.51	99.2				*47.76*	*46.45*		*46.57*	*43.46*	*46.76*
'SiO_2'	*50.19*	*46.68*									*52.24*	*53.55*		*53.43*	*56.54*	*53.24*
XRF-*INAA*	ppm															
Rb	*28*	*n.d.*	5	14	11	11	11	*45*	*3.7*	*n.d.*	*45*	*(71)*	*29*	*37*	*48*	*45*
Ba	*963*	*670*	379	500	400	561	739	*830*	*133*	*n.d.*	*917*	*1056*	*1142*	*1051*	*1087*	*1182*
Sr	*n.d.*	*n.d.*	366	377	424	366	351	*n.d.*	*514*	*n.d.*	*n.d.*	*n.d.*	*n.d.*	*n.d.*	*n.d.*	*n.d.*
Zr			100	144	127	101	153									
Nb			9.7	11.0	9.9	10.2	13.3									
Y			34	66	77	50	68									
Zn	*180*	*122*	209	335	328	120	161	*159*	*9*	*23*	*472*	*498*	*145*	*206*	*457*	*430*

Pb			4	10	12	8	14									
Ga			15	20	20	20	20									
V			234	235	207	222	430									
Cu			46	42	47	62	43									
Ni			101	44	44	103	50									
Cr	*96*	*100*	116	80	101	89	89	*92*	*11.6*	*3100*	*73*	*128*	*80*	*73*	*42*	*27*
INAA ppm																
Cs	0.63	0.65	0.37	5.74	4.99	0.42	0.47	0.54	0.11	0.08	1.68	2.53	0.99	1.11	2.86	1.62
Th	n.d.	1.37	0.50	0.60	0.49	0.78	1.21	1.00	0.11	n.d.	1.94	2.37	1.72	3.13	2.84	2.50
Hf	1.65	2.87	2.67	3.21	2.85	2.54	3.98	4.82	0.05	n.d.	5.08	6.56	4.80	6.00	8.20	7.21
Ta	0.37	0.45	0.45	0.59	0.46	0.50	0.73	0.75	0.03	n.d.	0.87	0.94	0.73	1.02	1.08	1.06
Sb	n.d.	0.74	0.48	0.55	0.69	0.43	0.47	0.50	0.15	n.d.	0.81	1.09	0.72	0.92	0.79	0.98
Sc	13.1	24.8	26.5	35.2	31.5	29.1	37.2	39.1	0.56	154	35.9	39.6	35.0	34.6	33.0	41.3
Co	21.6	52	36.1	24.1	24.3	48.1	31.3	31.4	0.9	37.7	24.1	22.7	20.4	19.7	16.6	19.2
La	11.9	33.1	14.2	22.6	21.9	18.6	25.0	24.7	2.44	1.2	33.2	35.3	22.9	30.3	36.8	34.2
Ce	20	57	35	48	45	41	49	56	3.5	5.9	74	80	51	77	86	77
Nd	12	42	21	34	35	27	33	38	n.d.	8.6	48	57	32	47	49	48
Sm	4.00	10.79	6.06	9.61	10.30	7.72	9.84	9.70	0.21	3.51	12.70	13.73	9.24	11.96	12.8	14.1
Eu	2.10	3.79	2.16	2.99	2.48	2.87	3.70	3.79	0.62	1.51	4.52	5.24	3.78	4.45	4.40	5.24
Tb	0.82	1.92	1.03	1.51	1.69	1.08	1.48	1.61	0.06	0.78	2.54	2.68	1.85	2.38	2.11	2.30
Dy	4.3	12.5									16.1	19.6		16.3	12.83	16.41
Yb	3.30	6.37	4.00	5.66	7.84	4.17	6.17	5.34	0.08	2.11	9.80	10.20	5.50	7.48	7.61	7.18
Lu	0.50	0.89	0.62	0.85	1.16	0.61	0.90	0.78	0.017	0.24	1.49	1.53	0.76	1.10	1.20	1.08

[a] See Streck (1994) for 9 additional dacite pumice analyses not reported here. Selected high-silica rhyolites span the range of compositions from most evolved rhyolite group A to least evolved group E (HSR-group) (Streck and Grunder 1997); group A: RT173H, group B: RT34E, group D: RT173B, and group E: RT173A. For mafic inclusions with mainly INAA data, P_2O_5 was determined by electron microprobe (EMP; number of averaged analyses shown in parentheses) and 'SiO_2' was calculated by mass balance. Mineralogy refers to phenocrysts, glomerocrysts, or major phases of cumulus inclusions. First number of inclusion identification refers to locality and capital letter indicates host pumice from which inclusion was extracted. HAOT basalt HP33 is slightly older and the others are slightly younger than Rattlesnake Tuff (see text). Analyses used for average dacite composite are: RT2A, -6D, -6E, -50A, -50B, -60A, -60B, -60D, -141A, -165C, -2101A, and -211A. Number in parentheses of average of crystal-poor inclusions (average xls-poor inclusion) is one standard deviation, in %, of the compositional spread. Mafic mixing endmember at 1:1 is the calculated composition of the mafic endmember necessary based on a model of equal amounts of mafic endmember and least evolved rhyolite (group E) of the Rattlesnake Tuff to produce average dacite. Note the similarity to the observed average composition of crystal-poor inclusions

[b] Phenocrysts or glomerocrysts

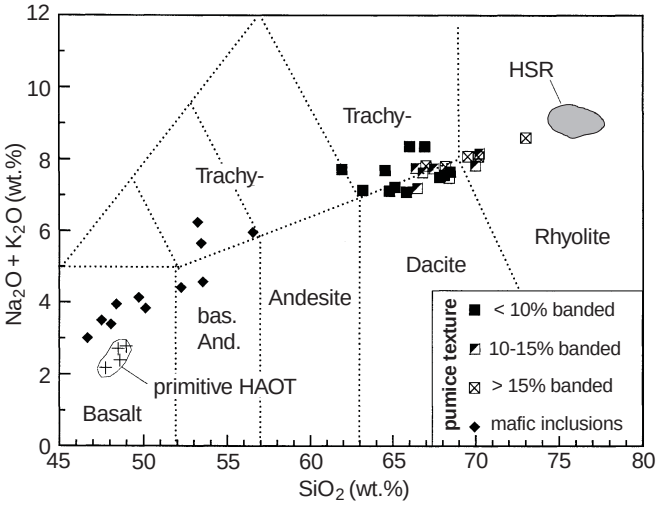

Fig. 2 Silica versus total alkalis for Rattlesnake Tuff samples and nearly coeval, primitive HAOT lavas (Table 1). HSR indicates the compositional field for Rattlesnake Tuff high-silica rhyolites; *squares* are for dacite pumices with different patterns to indicate the estimated volume of non-dacite bands. *Solid diamonds* represent analyses of mafic inclusions. For this and all other diagrams, major element data are normalized to 100% volatile free. Classification according to LeBas et al. (1986)

some inclusions are less than 3% for Mn, 5% for Al, Fe, K, and Ti, and 5–10% for Ca and Mg, as obtained during counting after short activation at a power level of 50 kW.

All mineral analyses and phosphorus concentrations of some basaltic inclusions were obtained by electron microprobe analysis. Minerals and glasses in inclusions were analyzed in polished sections and grain mounts on a Cameca SX-50 at Oregon State University and at GEOMAR, Kiel. Accelerating voltage was 15 kV and power level ranged from 15 to 30 nA.

Results: composition and mineralogy of basaltic inclusions and dacites

Basaltic inclusions

Basaltic inclusions range from basalt to basaltic andesite or to basaltic trachyandesite in composition (Fig. 2). Crystal-poor inclusions have high P_2O_5, MnO, TiO_2, alkali and incompatible trace elements concentrations coupled with low MgO, indicating that they are substantially more differentiated than primitive olivine tholeiites in the region (Fig. 4). Crystal-rich inclusions have compositions intermediate between crystal-poor inclusions and primitive olivine tholeiites. Some crystal-rich inclusions are affected by crystal accumulation and like cumulus inclusions, do not represent liquid compositions. High Al_2O_3, positive Eu anomaly ($Eu/Eu^* = 1.5$), and low $Fe_2O_3^*$ and Sc demonstrate plagioclase accumulation in inclusion 2A.i1. Taken together, mafic rocks of the Harney Basin and mafic inclusions in the Rattlesnake Tuff form a continuous compositional trend from primitive tholeiites to crystal-poor inclusions and so define a liquid line of descent (Table 1, Fig. 4).

Plagioclase compositions for all inclusions range between $\sim An_{80}$ to An_{50} (Fig. 5), with zonation of less than 6% An in individual crystals. The most calcic feldspars are phenocrysts in the crystal-rich inclusions and in cumulus inclusions. Plagioclase of $An_{35–30}$ is associated with Fo_{22} olivines (cf., McBirney 1996).

The majority of clinopyroxene phenocrysts are slightly corroded, but retain part of their euhedral shape (Figs. 3g, i). Clinopyroxene in crystal-rich inclusion 2101exi and isolated basaltic clinopyroxenes are $Wo_{42}En_{45}Fs_{13}$ to $Wo_{37}En_{42}Fs_{21}$ and Cr ranges from 0.45 to <0.1 wt% (Table 2, Fig. 5c). Poikilitic augites, in contrast, have restricted compositions around $Wo_{42}En_{45}Fs_{13}$ and contain ca. 0.4 wt% Cr_2O_3. One corroded orthopyroxene crystal in dacite is $Wo_4En_{71}Fs_{25}$ and most likely originated from basaltic magma.

Olivine in inclusions ranges from fresh to completely altered to iddingsite within single host pumices. Fresh olivines range from Fo_{81} to Fo_{72}, but in some cumulus inclusions they are Fe-hortonolite ($Fo_{23–22}$) (Fig. 5d). Single euhedral olivine crystals entrained in dacite compositionally overlap with olivine from glomeroporphyritic olivine-plagioclase inclusions, but most are slightly less magnesian (Figs. 5d, 6).

Dacites

Most dacite pumices are banded, so care was taken to select homogeneous parts for major and trace-element analysis through hand-crushing and selecting lapilli-size pieces. Some of the non-dacite material could not be removed and its volume percent is estimated (Table 1). Some strongly banded pumices were analyzed as well. Silica concentrations range from 62 to 73 wt% for all dacites, but only 62–68 wt% if strongly banded pumices are excluded. Dacite glass analyses by electron microprobe range from 66 to 68 wt% SiO_2 and likely reflect equilibrated compositions (albeit, microprobe analyses are hindered by microlites.). Excluding clearly commingled pumices, compositional gaps of about 7 and 8 wt% SiO_2 separate dacite pumices from high-silica rhyolite pumices and basaltic inclusions, respectively, and significant compositional gaps occur in many other element distributions (Figs. 2, 4).

Dacites are subalkaline to mildly alkalic (Fig. 2) and have an icelanditic character indicated by FeO*/(FeO* + MgO) that ranges between 0.76 and 0.81 (Table 1), near the transition between calc-alkaline and tholeiitic rocks. Major element correlations and the variations of Sc, Co, and Sr with major elements are mainly linear (Fig. 4). Some incompatible trace elements variations, e.g., La, Ba, and Ta, are scattered.

Dacites contain about 1 to 5 vol.% crystals. Heavy-liquid mineral separates on two samples yielded 1.2 and 2.4 wt% minerals. Even in pumices with little banding, mineral assemblages are strongly bimodal with one population like those in high-silica rhyolites and another like those in basaltic magma (Fig. 5, Table 2). Many

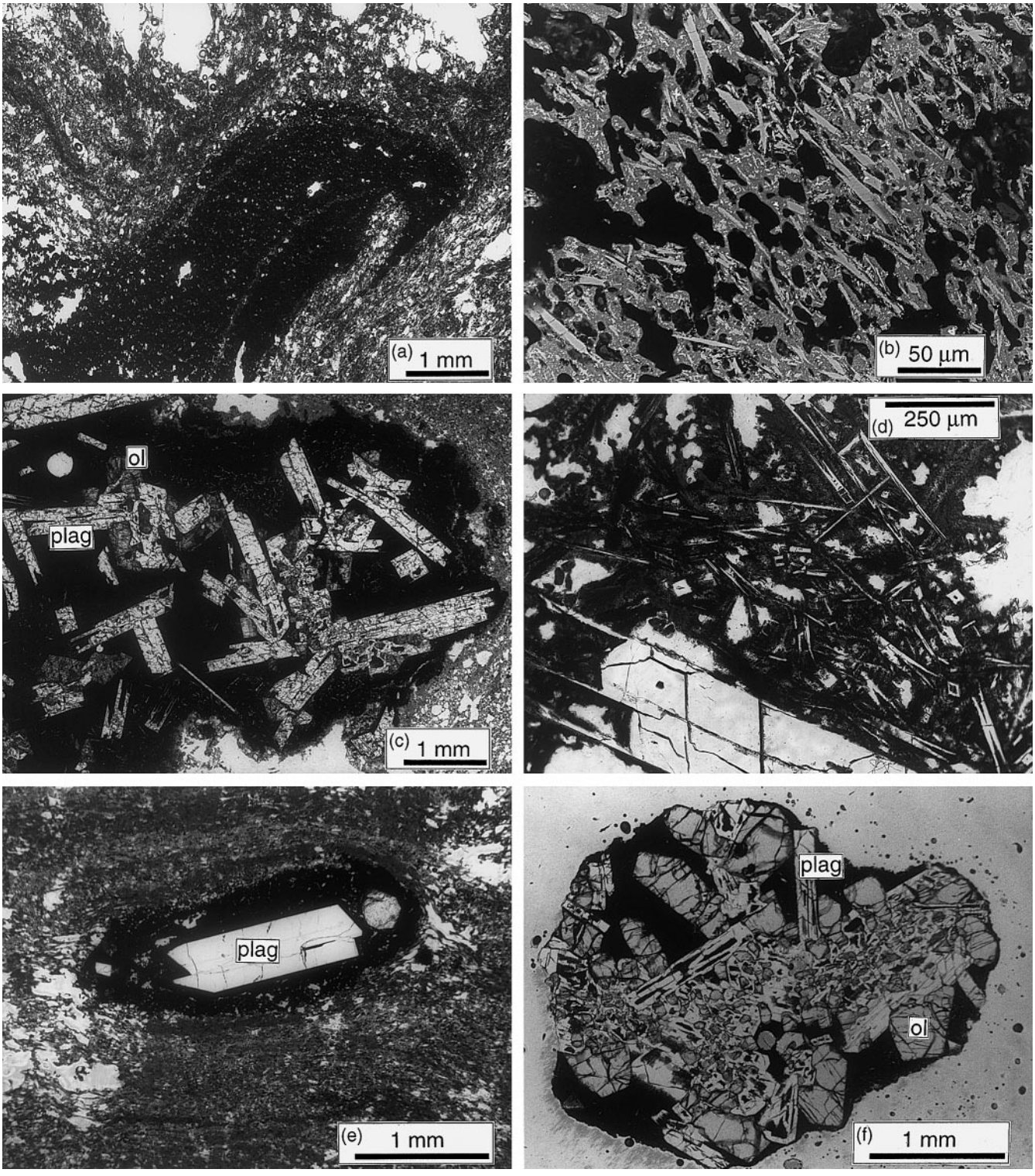

Fig. 3 (see page 203 for legend)

crystals are enclosed in blobs or selvages of high-silica rhyolite or basaltic groundmass further confirming that they are entrained relicts in a commingled magma. The isolated rhyolitic and basaltic phenocrysts may be euhedral or have signs of disequilibrium such as resorption features or reaction rims. The existence of true dacite, not merely commingled basalt plus rhyolite, is confirmed by the presence of virtually homogeneous dacite clasts and phenocrysts that are not attributable to either a rhyolite or basalt source, that is, dacitic phenocrysts. Such phenocrysts are rare and include augite ($En_{26–33}$ Wo_{37}) and probably plagioclase ($An_{30–50}$) (Fig. 5, Table 2).

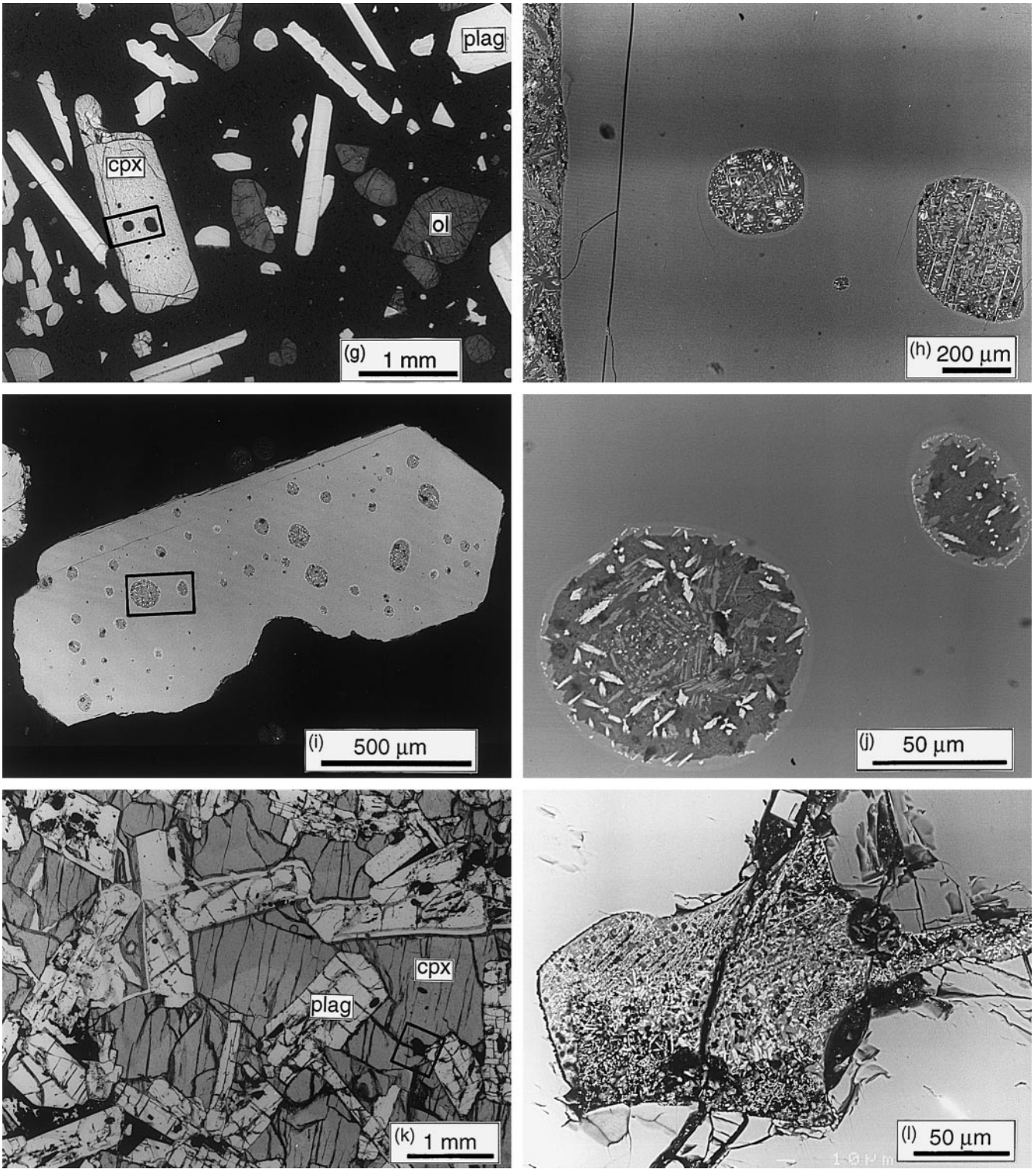

Discussion

Mafic inclusions in the Rattlesnake Tuff are a critical record of the hidden mafic underpinnings of this large silicic volcanic center and thereby are a record of the interaction of basalt with the crust. The discussion is structured to first consider the composition of the mafic inclusions compared to regional basalt and then to examine the petrologic relationships among them. Finally, we treat the origin of dacites and the nature of the mafic-silicic interface.

◄

Fig. 3a–l Images of mafic inclusions, (**a**, **c**, **d**, **e**, **f**, **g**, and **k** under plane polarized light; **h** in reflected light; **b**, **i**, **j** and **l** are backscattered electron images). Labels on pictures are *ol* for olivine, *cpx* for clinopyroxene, and *plag* for plagioclase. Close-up areas in **g**, **i** and **k** are marked by *rectangles*. **a** Part of crystal-poor inclusion #116B.i1 (*black*) shows mingling texture with host pumice #RT116B. **b** Quenched groundmass of crystal-poor inclusion #106A.i1; *lightest areas* with spiny texture are mainly quenched clinopyroxene crystals in *medium-gray* glass. *Black* areas are mainly vesicles. **c** Glomeroporphyritic olivine (Fo_{79}) and plagioclase in crystal-rich inclusion #14D.i1 with crenulate margin; some plagioclase phenocrysts have hopper texture. **d** Hopper texture of phenocrysts ($An_{70–76}$) in crystal-rich, olivine-plagioclase inclusion #2A.i1. **e** Quenched basaltic selvage (*black*) around plagioclase and olivine (Fo_{75}) crystals in dacite pumice. **f** Very crystal-rich, olivine (Fo_{80}) – plagioclase inclusion. **g** Crystal-rich inclusion #2101exi with olivine, clinopyroxene and plagioclase phenocrysts. **h** Close up of part of **g** showing quenched groundmass and melt inclusion around and in clinopyroxene ($Wo_{42}En_{44}Fs_{14}$) **i** Single, formerly euhedral, slightly corroded basaltic clinopyroxene ($Wo_{38}En_{44}Fs_{18}$) with abundant melt inclusions found in dacite. **j** Close up of melt inclusions in **i** showing quenched crystals surrounded by remaining glass (*dark*). **k** Cumulus inclusion with cpx ($Wo_{42}En_{45}Fs_{13}$) – plagioclase; *black* is quenched interstitial liquid. **l** Close-up of interstitial liquid pocket from lower right hand corner of **k** indicates rapid chilling through spiny quench crystal formation

Regional and local basalts

The ambient mafic input into the crust is well known in the northwestern Great Basin, including the Harney Basin. Basalts younger than about 11 Ma are high alumina olivine tholeiites (HAOT) (e.g., Hart et al. 1984) that contain sparse phenocrysts of olivine of $Fo_{68–88}$ and commonly plagioclase of An_{60} to An_{86} (Hart et al. 1984; Grove et al. 1988; Draper 1991; Baker et al. 1991). The most primitive HAOT have geochemical characteristics akin to mid-ocean-ridge basalts and back-arc basin basalts, such as high MgO/FeO* at MgO concentrations commonly of 8 to 10 wt% and low K_2O and Rb (< 0.3 wt%, 1–4 ppm, respectively) (Carlson and Hart 1981; McKee et al. 1983; Hart et al. 1984; Grove et al. 1988; Draper 1991; Donnelly-Nolan et al. 1991; Bailey and Conrey 1992). The most primitive of these were in equilibrium with a mantle assemblage of olivine, augite, plagioclase, spinel, and orthopyroxene at about 1.1 GPa (Bartels et al. 1991; Draper 1991).

In the Harney Basin, sparse age determinations on basalts range from ~8 to ~3 Ma (Parker 1974; Walker 1979; Streck and Grunder unpublished data). Primitive HAOT erupted during the life cycle of the Rattlesnake Tuff magma chamber, but apparently peripherally to the rhyolite magma chamber (cf., Valentine 1993). Forty km south of the tuff's vent area, the tuff overlies the unweathered pahoehoe surface of a primitive HAOT lava (sample HP-33) and underlies a basalt (93.1ba) that is itself capped by the 6.8-Ma tuff of Buckaroo Lake (Figs. 1, 2, Table 1 ; Grunder unpublished data). At the same location, several basalt sills compositionally like the overlying basalt (e.g., sample MiSi) intrude the Rattlesnake Tuff.

Range of basaltic compositions sampled by mafic inclusions

The composition of basaltic magmas that existed under the Rattlesnake magma chamber can be inferred directly from the composition of the crystal-poor mafic inclusions and also indirectly from the composition of isolated and cumulus minerals.

Inferred compositions range from high-MgO basalts to advanced tholeiitic fractionation products like FeTi basalts to basaltic andesites. The overall magma evolution of the mafic inclusions follows a mild iron-enrichment trend along with enrichment of TiO_2, MnO, P_2O_5, and Zn (Fig. 4) (cf., Carmichael et al. 1974; Naslund 1989). Crystal-poor, basaltic andesite inclusions are moderately (3x) to strongly (20x) enriched in incompatible elements, particularly K, Rb, Ba, Ta, rare earth elements (REE), Hf, but only moderately depleted (≥0.2x) in compatible elements compared to primitive HAOT (Table 1, Figs. 4, 7a). Crystal-rich inclusions have compositions between HAOT and crystal-poor inclusions (Fig. 4). Incompatible trace-element enrichment combined with a mild iron-enrichment trend is also recorded by mafic inclusions from other tuffs, e.g., from the voluminous rhyolitic Oruanui Tuff, New Zealand (Sutton et al. 1995).

Mg-rich olivines ($Fo_{78–81}$) in inclusions are evidence for basaltic liquids with magnesium numbers [Mg#, molar $Mg/(Mg + Fe^{2+}) \times 100$] of 54 to 56, which overlap with values for high-MgO Harney Basin basalts (MgO > 7 wt%) (Fig. 6a). All isolated olivines and some olivines from inclusions reflect equilibrium with slightly lower Mg# liquids and overlap with the upper range for whole-rock analyses of crystal-poor inclusions. Calculated Ni concentrations of liquids in equilibrium with inclusion olivine similarly yield values that overlap with Harney Basin high-MgO basalts (Fig. 6b).

The presence of some high-Cr augites (0.2–0.4 wt% Cr_2O_3), as isolated crystals or in cumulus inclusions, further indicates crystallization from a more primitive, Cr-rich basalt magma. Using D_{Cr} of ~10 for clinopyroxene (Skulski et al. 1994), calculated Cr concentrations in melts completely overlap with compositions of local HAOT lavas. Using D_{Cr} of 4 (Hart and Dunn 1993; Hauri et al. 1994) yields compositions more enriched in Cr (Fig. 6c). Two plagioclase-olivine inclusions contain a few high-Cr augites as phenocrysts (Fig. 3g) indicating that the high-Cr basalt recorded by clinopyroxenes is on a liquid line of descent from the high-MgO, high-Ni basalt recorded by olivines.

Finally, evidence for extreme differentiation along a tholeiitic trend lies in Fe-hortonolites from two cumulus olivine-plagioclase inclusions (cf., McBirney 1996). These are mineralogically distinctly different from minerals of HAOT lavas but are similar to olivines from a nearby basaltic trachyandesite cone (Paiute Butte, formerly Squaw Butte, MacLean 1994) (Fig. 1).

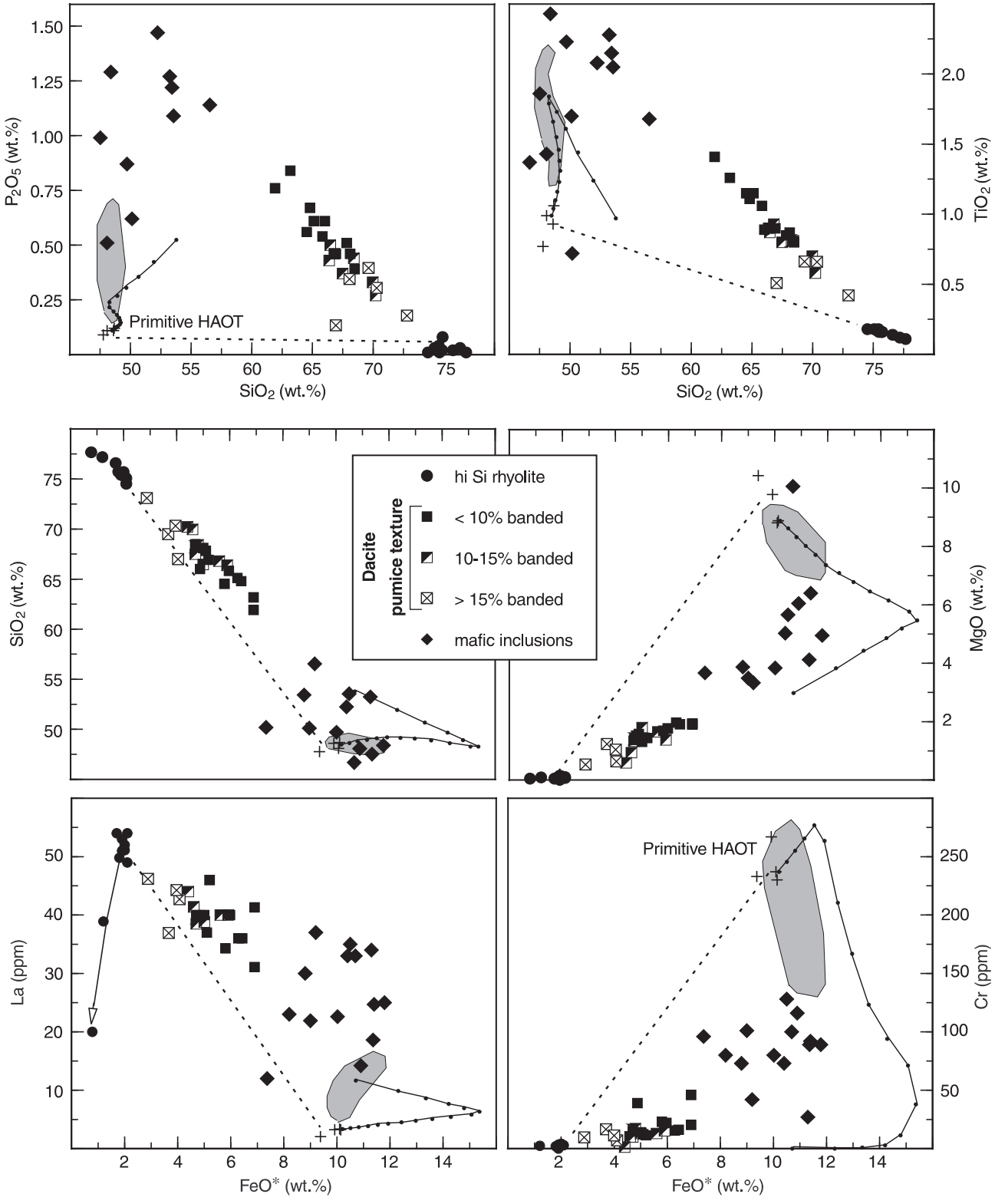

Derivation of compositionally evolved basaltic inclusion magma

Major and trace element modeling was done to examine the liquid line of descent beginning with HAOT, evolving along the trend of crystal-rich and crystal-poor inclusions and culminating in the most incompatible element-enriched crystal-poor inclusions (Fig. 7). The crux of the modeling problem is that the basaltic andesites are strongly enriched in incompatible

◀

Fig. 4 Variation diagrams of Rattlesnake Tuff samples (see symbol key) (Table 1). *Crosses* are primitive HAOT lavas close in age to the Rattlesnake Tuff. *Gray field* includes 14 other Harney Basin HAOT with MgO ≥7 wt%. *Dotted lines* are hypothetical mixing lines between primitive regional basalt and least evolved Rattlesnake Tuff high-silica rhyolite. *Solid lines* with tick marks are crystal fractionation trends calculated with program COMAGMAT (Ariskin et al. 1993) using HAOT sample 93.1ba (Table 1) as parent composition; *tick marks* are at 5% crystallization intervals; other input variables for COMAGMAT model were: pressure = 4 kb, H_2O = 0.15 wt%, oxygen buffer = FMQ. *Solid line with arrow* indicates fractionation trend within Rattlesnake Tuff high-silica rhyolites (Streck and Grunder 1997)

elements, but have mafic bulk composition and are only moderately depleted in compatible trace elements. We here detail trade-offs between crystal fractionation, assimilation, and mafic recharge in modeling the observed trends.

Major-element compositions, mineral modes and mineral compositions were calculated with the forward model COMAGMAT (Ariskin et al. 1993). Trace element concentrations were calculated using inputs consistent with the major element models (modes, degrees of crystallization, amount of assimilation or recharge) and published partition coefficients (Table 3). The basaltic parent and the mafic recharge composition is 93.1ba and the silicic contaminant is least evolved rhyolite E (Table 1). Crystallization conditions were chosen at P = 0.4 GPa at the FMQ buffer and with initial water at 0.15 wt%. The pressure and water input was selected to produce results consistent with coexistence of augite and olivine in fairly magnesian bulk compositions and to suppress plagioclase crystallization slightly. Models for basaltic andesites (Fig. 7) range from fractionation or assimilation (mixing) alone, to fractionation combined with recharge, to fractionation combined with recharge and assimilation.

The models including fractionation (models A, C, D, E) predict mineral compositions almost identical to those observed (Fig. 7d). All models underpredict Ti concentrations mainly because COMAGMAT seems to predict crystallization of spinel too early, as observed by Yang et al. (1996). While no model produces a perfect fit, pure fractionation (model A – Fig. 7, 4) produces compositions too high in Fe, too low in K and P, and mostly much too low in incompatible trace elements, yielding a compositional pattern that is too flat (Fig. 7b). Pure assimilation (model B) results in incompatible trace-element concentrations, Fe and P that are low to much too low.

Fractionation combined with recharge (model C) is more successful at producing incompatible element enrichments without strong compatible element depletion, but the resultant trace-element pattern is too flat; also K and Al are too high. One fractionation and recharge cycle in model C includes 50% crystal fractionation (Fig. 7) followed by mixing of the remaining daughter with parental basalt to recover to the original magma volume. In general, the degree of fractionation is con-

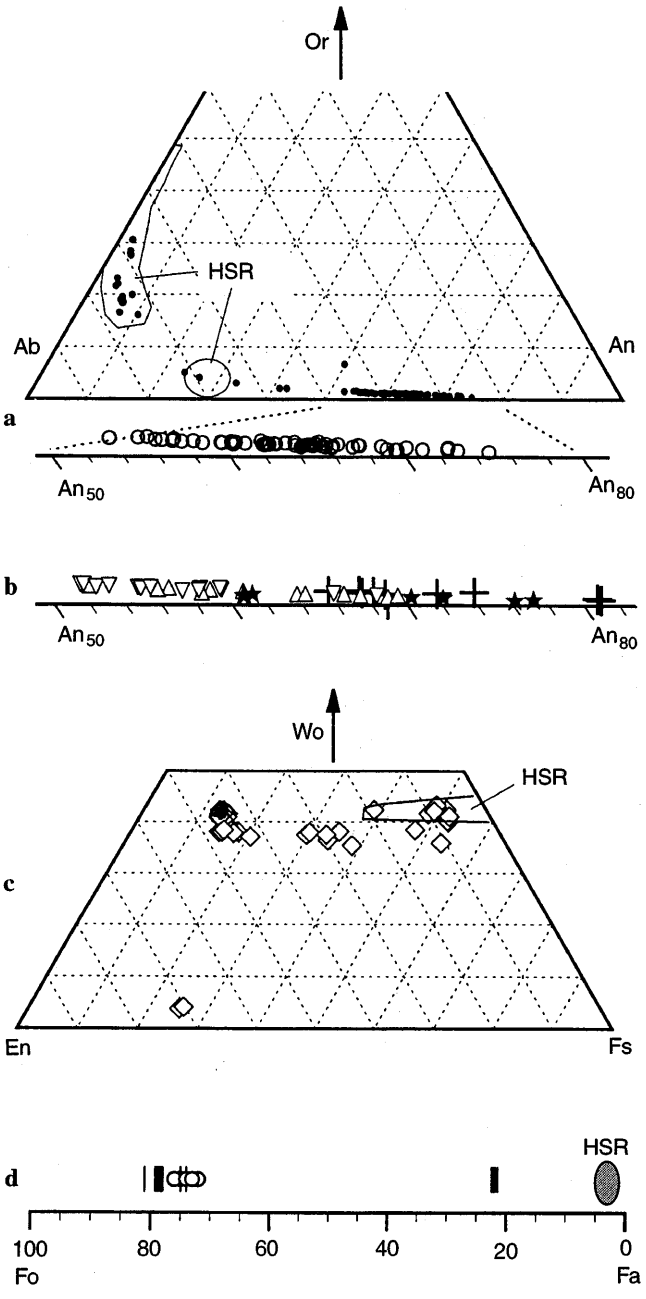

Fig. 5a–d Electron microprobe data projected as mol%. Each point represents one analysis. See Table 2 for representative mineral analyses. Fields indicate mineral compositions of high-silica rhyolites (HSR). The field for HSR-andesines is uncertain because such phenocrysts are only in the most evolved rhyolite (rhyolite A) and are extremely sparse (Streck and Grunder 1997). **a** Feldspar compositions in dacites. **b** Feldspar compositions in mafic inclusions. *Stars* indicate feldspars from crystal-rich olivine-plagioclase inclusion #2A.i1 (*stars* at lower An are for groundmass crystals); *crosses* represent two cumulus cpx-plagioclase inclusions; *triangles* are crystal-poor inclusions, and *inverted triangles* are single basaltic phenocrysts surrounded by mafic selvages. Not shown are An_{30-35} feldspars associated with Fo_{20} olivines (ferrohortonolites). **c** Pyroxene compositions. *Open diamonds* indicate pyroxene crystals in dacite pumices; *solid dots* are pyroxene compositions of crystal-rich and cumulus cpx-plagioclase inclusions. **d** Olivine compositions; *vertical bars* represent olivine in mafic inclusions and *open circles* represents compositions of single crystals or glomerocrysts consisting of < 5 grains found in dacite pumices

Table 2 Representative mineral analyses. (Fe_2O_3 by charge balance, *n.d.* not detected, – not analyzed. Sample indicates pumice or inclusion #. Location of analysis of single grains is indicated by: *ctr* center of grain, *hlf* halfway, *rim* near but not directly at rim of grain)

	High-silica rhyolites				Mafic inclusions				Dacites		
Sample	*RT34E*	*RT173B*		*RT34C*	*2A.i1*	*210B.i12*	*60*X.i1	*55i1*		*RT210.1B*	*RT210.1B*
Feldspar	ctr	hlf		hlf	ctr	ctr				ctr	hlf
SiO_2	66.06	65.32		65.27	48.52	60.01	50.92	51.05		50.38	54.59
Al_2O_3	19.05	20.05		20.54	32.26	24.94	30.97	31.29		30.55	27.88
FeO	0.20	0.21		0.21	0.58	0.35	0.62	0.66		0.65	0.59
CaO	0.19	0.63		1.13	15.57	6.60	13.75	13.74		13.38	10.59
Na_2O	5.78	7.55		8.07	2.53	7.55	3.42	3.43		3.82	5.17
K_2O	8.13	4.62		3.27	0.08	0.54	0.14	–		0.15	0.25
BaO	0.28	1.37		1.51	n.d.	–	–	–		0.06	0.04
Total	99.69	99.74		99.99	99.66	99.99	99.90	100.34		99.08	99.22
An	0.9	3.2		5.8	76.9	31.6	68.4	68		65.3	52.3
Ab	51.4	69.0		74.4	22.6	65.3	30.9	32		33.8	46.2
Or	47.6	27.8		19.8	0.4	3.1	0.8	–		0.9	1.5
Sample	*RT34E*	*RT173B*	*RT173B*	*RT34C*	*14D.i1*	*210B.i12*	*60X.i1*	*55.i1*	*RT2A*	*RT210.1B*	*RT210.1B*
Pyx/oliv	ctr	ctr	ctr	hlf	rim	hlf			ctr	rim	rim
SiO_2	49.37	47.84	29.34	48.11	38.7	31.18	50.44	50.35	51.25	49.98	37.54
TiO_2	0.17	0.26	0.02	0.24	0.02	0.02	1.07	1.13	0.50	1.08	0.01
Al_2O_3	0.38	0.37	0.01	0.37	0.02	n.d.	3.34	4.16	1.22	3.62	0.04
Cr_2O_3	n.d.	n.d.	–	n.d.	–	–	0.47	0.47	n.d.	0.39	–
Fe_2O_3	2.38	2.21	–	1.10	–	–	–	–	0.15	–	–
FeO	19.09	25.76	63.33	26.63	19.43	56.67	7.73	7.65	17.63	8.27	21.77
MnO	3.29	2.4	5.44	2.4	0.32	2.5	0.19	0.2	1.26	0.24	0.38
MgO	6.10	2.37	1.51	2.17	41.59	9.18	15.53	15.00	10.61	15.34	39.55
CaO	17.82	17.59	0.29	17.75	0.28	0.21	19.82	20.62	17.48	20.24	0.24
Na_2O	0.66	0.54	–	0.44	–	–	0.44	0.45	0.33	0.41	–
Total	99.25	99.34	100.23	99.24	100.45	99.79	99.08	100.03	100.43	99.57	99.74
Wo	40.7	41.0		41.0			41.8	43	37.2	42	
En	19.4	7.7		4.9			45.5	44	31.4	44	
Fs	39.9	51.3		54.1			12.7	13	31.4	14	
Fo			3.8		79	21					76
Fa + Te			96.2		21	79					24

strained to fall between the onset of clinopyroxene and subsequent Fe-Ti oxide crystallization, in order to maintain mafic bulk composition.

Finally the two models which combine fractionation and recharge, with assimilation (model D & E) provide the best overall fits to observed data because mafic bulk composition is maintained, incompatible elements are enriched overall, and a tilted trace element pattern is imparted by the silicic contaminant. Predicted Al and K remain high. In model E, 2–4% assimilation occurs continuously during each fractionation and recharge cycle. In model D, the same 30% rhyolite is assimilated, but all at the end of last cycle (Fig. 7). Model E matches slightly better with the data. The important difference between the models that include assimilation and those that do not, is that less mafic magma is required, owing either to fewer recharge cycles (D) or less fractionation (E).

Substantial mafic recharge is essential in any model in order to prevent silica enrichment. The importance of recharge is emphasized by the covariation of Co and Ta (Fig. 8). Recharge offsets the strong depletion in Co and prevents the silica enrichment that would occur if fractionation or assimilation of silicic contaminant were the main means of Ta enrichment. Recharge can also prevent Fe-Ti oxide saturation, which would drive strong silica enrichment. Recharge models simulate observed compositions unless recharge is combined with assimilation of compositions enriched in trace elements by extreme ($\geq 95\%$) fractionation (see "9:1 recharge model" in Fig. 8).

In summary, we attribute most of the enrichment in incompatible elements of the inclusions to extensive crystal fractionation from HAOT, while keeping the bulk composition basaltic and compatible elements only moderately depleted through recharge with primitive HAOT. Some assimilation, e.g., of a rhyolitic contaminant, has to be included to account for differential enrichment of the incompatible trace elements.

Dacites: mafic-silicic interface

Dacite in the Rattlesnake Tuff was formed by simple mixing between the least evolved rhyolite and basaltic andesite rather than typical HAOT. Evidence includes

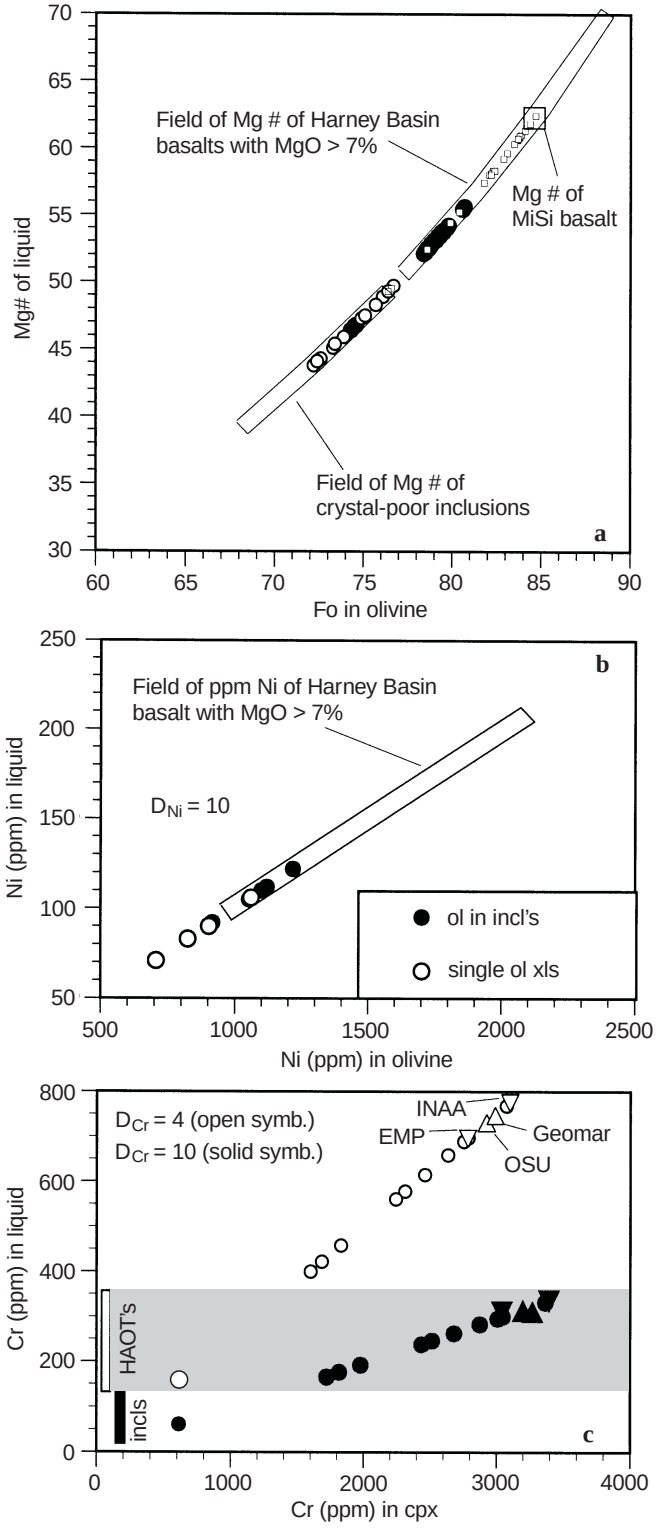

◄

Fig. 6a–c Mineral compositional data from mafic inclusions compared to real and calculated basaltic liquids. **a** Mg# versus Fo: inclusion legend as in panel b. Mg# of the liquid is calculated based on measured Fo content of olivine, assuming that X_{Fo}/X_{Mg} of olivine relative to melt = 0.3 (Roeder and Emslie 1970) and that all Fe is FeO. *Small squares* are olivine data and *large square* represents bulk compositional data of HAOT sample MiSi (Table 1). **b** Ni concentration of olivine relative to liquid based on a partition coefficient (D) of 10 for Ni in olivine (cf., Green 1994). **c** Cr concentrations of clinopyroxene compared to calculated melt concentrations with D = 4 and D = 10. *Circles* for clinopyroxene phenocrysts; *triangles* for clinopyroxene of one cumulus inclusion obtained by microprobe at Oregon State Univ. and at GEOMAR Research Center, and *inverted triangles* for Cr data of clinopyroxene from cumulus inclusion 60X.i1 (Table 1) by two analytical methods (EMP = electron microprobe, INAA = instrumental neutron activation analysis), (see text); bars along y-axis indicate observed range of Cr concentrations of HAOT lavas and Rattlesnake Tuff mafic inclusions (incls.); calculated liquid Cr concentrations overlap with observed Cr concentrations of HAOT samples in shaded region

the bimodal, basaltic-rhyolitic, crystal assemblage of the dacite (Fig. 5) and the compositional colinearity of crystal-poor inclusions with dacite and least-evolved rhyolite (Figs. 2, 4). Dacites fall far from a mixing line between regional basalt (HAOT) and rhyolite (Fig. 4) and such a model is not considered further.

To evaluate the mixing hypothesis, we calculated the mixing proportions of rhyolite and basaltic andesite necessary to match observed compositions of dacites with less than 10% banding. We used both average and individual dacite analyses (Fig. 9). The mafic mixing component is a composite of the crystal-poor inclusions and the silicic component is rhyolite from the Rattlesnake Tuff. We limited the test to those elements for which one standard deviation of the average basaltic andesite composite is ≤20% (Table 1). Na was excluded because its concentrations are too variable in the rhyolites owing to post-eruptive processes (Streck and Grunder 1997).

About equal proportions of rhyolite and basaltic andesite yield a good match for average dacite for most elements. Proportions of rhyolite necessary to match individual pumice analyses vary from about 35 to 65% (Fig. 9b). The choice of rhyolite makes little difference in the resultant mixing proportions, but matches are best with least-evolved rhyolite E (Fig. 9a).

Some trace elements require a mixing proportion much different from other elements or have concentrations that are slightly outside the range of the end members and so have no mixing solution. For mixtures with rhyolite E (Fig. 9b), Ta, Hf, Eu concentrations in the dacites typically require too much rhyolite or have no mixing solution. Ba and La (LREE) require more basaltic material than dictated by other elements. Sm and Tb (MREE) concentrations are commonly slightly lower in dacites than in either end member (Table 1). Reasons for these discrepancies may include some accumulation of basaltic or rhyolitic phenocrysts; for example, accumulation of basaltic plagioclase in dacite decreases Eu, requiring more rhyolite, and decreases the Ba concentration, requiring more of the mafic component. Also, differential diffusivities are likely to have some effect on magmas formed at the mafic-silicic interface (Watson 1976; Blichert-Toft et al. 1992). Despite these discrepancies, we emphasize that overall the fits are excellent. The average composition of crystal-poor inclusions

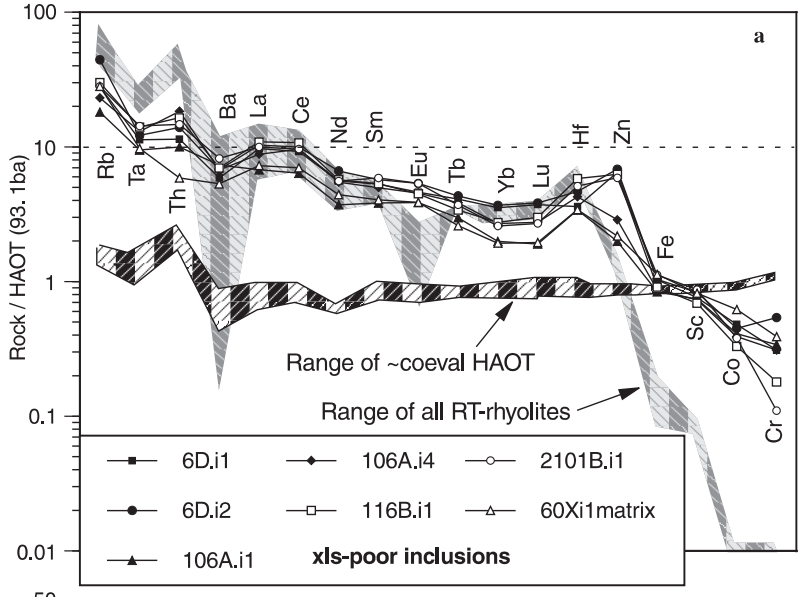

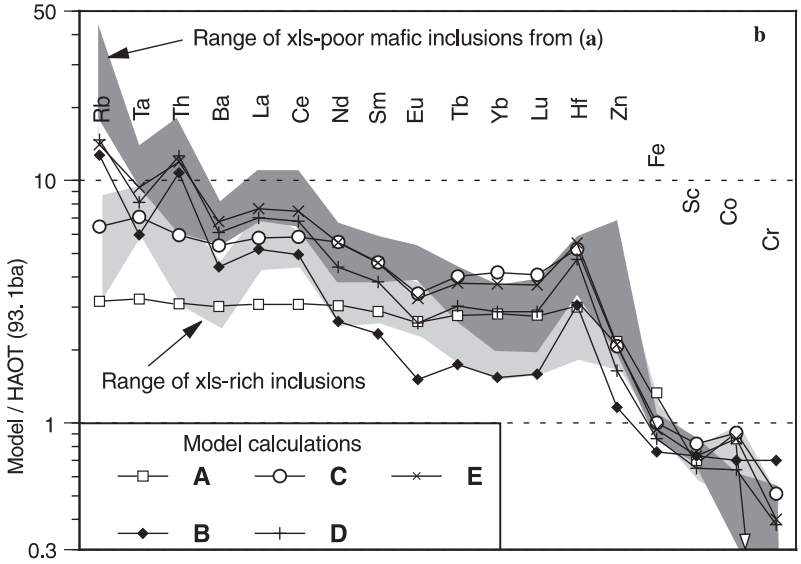

d

	Mineral composition modeled by COMAGMAT				Observed in all inclus. & isolated basalt. phenocyrsts
	A	C	D	E	
An-plag	81–55	–46	as in model C	–55	81-51,35-30
Fo-oliv	85–69	–75		–76	81–72, 22
En-cpx	47–42	–43		–43	46–42
Fs-cpx	10–19	–20		–18	12–19
Wo-cpx	43–39	–37		–39	45–38
En-opx	72–67	–68		–67	71
Fs-opx	21–26	–25		–26	25
Wo-opx	7–6.7	–6.5		–6.6	4

c

	Major element composition of model calculations					avg. xls-poor inclu.
	A	B	C	D	E	
SiO_2	50.9	56.1	50.0	56.7	52.9	53.8
TiO_2	1.45	0.74	1.06	0.95	1.07	2.05
Al_2O_3	16.1	15.3	17.2	15.0	17.4	14.4
FeO*	13.2	7.6	10.0	8.6	9.4	9.7
MgO	4.4	6.2	6.0	4.8	4.9	4.4
CaO	8.5	8.3	9.0	7.4	7.5	7.3
Na_2O	4.1	3.0	3.5	3.4	3.6	3.6
K_2O	0.75	1.54	1.67	2.06	2.28	1.48
P_2O_5	0.36	0.09	0.94	0.37	0.63	1.24

model	%fractionation	HAOT recharge cycles	mix. with HSR-E	frac. mode: oliv	plag	cpx	opx	mag
A:	70%	–	–	12.3	50.5	29.2	3.3	3.9
B:	–	–	30%			–		
C:	50%	14; 50%	–	1st: 16.1	56.3	23.5	4.0	0.0
D:	50%, 30% at end	10; 50%, 30% at end	30% at end	2nd-9th: 6.7	51.3	27.3	8.7	5.8
				10-14th: 8.8	51.5	30.7	3.3	5.6
E:	1st:50%, rest:40%	14;1st:50%, 40%	2% per cycle, 4% at end	2nd-7th: 3.0	49.6	29.412.7		5.3
				8-14th: 5.2	49.6	32.5	7.6	5.0

matches well with the calculated composition of the mafic end member required to be consistent with a 1:1 mix with rhyolite to produce average dacite (Table 1).

Subequal mixing proportions of mafic and silicic components have been found for intermediate igneous rocks in other systems (e.g., Frost and Mahood 1987; Feeley and Grunder 1991) and are controlled mainly by viscosity contrast between mafic and silicic magmas (Sparks and Marshall 1986; Frost and Mahood 1987). Viscosity-controlled mixing proportions are likely to be the cause for a compositional gap between hybrid dacite and high-silica rhyolite in the Rattlesnake Tuff (cf., Grove and Donnelly-Nolan 1986; Hildreth 1987; Bacon and Druitt 1988; Boden 1989; Brophy et al. 1996).

The degree of equilibration of the dacites can be used as a qualitative gauge of the degree of interaction between

◄

Fig. 7a–d Comparison of major and trace element data (**a**, **b**, **c**) and mineral compositions (**d**) of mafic inclusions with those predicted by five petrologic models (A, B, C, D, E; see text for discussion). Each model represents the best-fit calculated results for the specific modeling scenario. Model A is crystal fractionation alone. Model B is mixing with rhyolite only. Model C is fractionation combined with mafic recharge; the number of cycles of recharge and fractionation is indicated in the figure along with the percent of crystallization and the percent of recharge. Model D is fractionation combined with recharge cycles and with rhyolite contamination occurring once in the last cycle. Model E is fractionation combined with recharge cycles and with rhyolite contamination occurring at each cycle and at the end. The mode and amount of fractionation in the first cycle is identical in models C, D, and E; subsequent cycles in model D and E have less fractionation. See the lowest panel for details on percentages of each process and fractionating modes. **a** Compositional data of crystal-poor mafic inclusions normalized to primitive HAOT #93.1ba (Table 1). Range of ~coeval HAOT lavas is shown by *down-to-the-left ruled field*, which includes all basalts of Fig. 2. The range for all Rattlesnake Tuff high-silica rhyolites is shown by dark *down-to-the-right ruled field*. **b** Predicted concentrations of trace element models normalized to primitive HAOT #93.1ba; see Table 3 for partition coefficients used. Range of crystal-poor inclusions from **a** shown as *dark stippled field* and range of crystal-rich inclusions by *lighter stippled field*. Average mineral assemblages, based on results from COMAGMAT models, were used for modeling of trace elements; for models with recharge, C, D and E, three different average mineral assemblages were used to account for changing mineral proportions from first to last (xth) fractionation cycle. **c** Major element composition of models and of average crystal-poor inclusion (avg. xls-poor inclu.); B_2O_5 during fractionation was modeled as a perfectly incompatible element. **d** Mineral compositions predicted by models and observed in all inclusion and all isolated basaltic phenocrysts; for model C and E, the left boundary is the one of model A; *An-plag* is anorthite content of plagioclase, *Fo-oliv* is forsterite content of olivine, *En*, *Fs*, *Wo* refers to the enstatite, ferrosilite, and wollastonite component of clinopyroxene (*cpx*) and low-Ca pyroxene (*opx*)

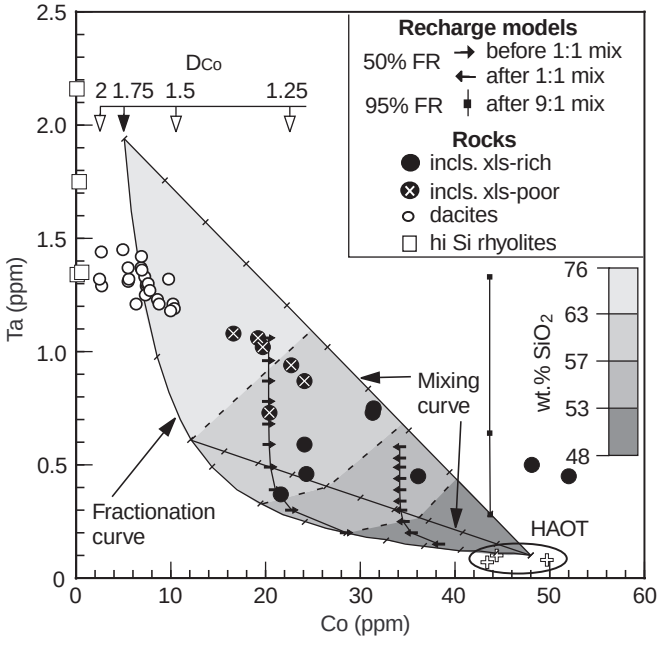

Fig. 8 Co–Ta variation diagram of Rattlesnake Tuff ejecta (see inset legend) compared to HAOT compositions (*encircled crosses*) and calculated chemical models of fractionation, mixing, and fractionation with mafic recharge. Diagram is contoured for silica values between fractionation and mixing curves; silica ranges apply only to models of mixing, fractionation or their combination. SiO_2 weight % of 53, 57, 63, and 76 along fractionation curve correspond with ~50, ~70, ~85 and ~95% fractionation, respectively, and were taken from Wright and Fiske (1971) in combination with Peck et al. (1966). Compositional spread of Rattlesnake Tuff mafic inclusions is too mafic to be explained by fractionation processes alone, mixing with silicic contaminant, or a combination of both. Inclusions would be required to have silica values mainly between ~57 to ~63 as opposed to observed silica values ranging mainly between ~50 and ~54 (Table 1). A mafic recharge model that includes 50% fractionation and basaltic recharge can explain inclusion data; model curves pass through data points while buffering silica at basaltic values (cf., Fig. 7c, model C). *Tick marks* along mixing and fractionation curves are at 10% intervals, except for 5% intervals above 80% fractionation. Calculated Rayleigh fractionation curve is based on a bulk $D_{Ta} = 0.01$ and $D_{Co} = 1.75$. If instead bulk D_{Co} values of 2, 1.5 and 1.25 are used, hollow *arrows* indicate the endpoint of the fractionation curve. Abbreviations and symbols in legend are: *%FR* = amount of fractionation; *after* versus *before* mix track the composition of the calculated model after or before mixing of the mafic magma with rhyolite at 1:1 or 9:1 proportions, respectively. Symbols on curves of recharge models represent successive cycles

Table 3 Partition coefficients used for models in Fig. 2 and 7 are within ranges for basaltic systems based on partition coefficients calculated from one cumulus inclusion (Table 1c) and published coefficients (Hart and Dunn 1993; Green 1994; Hauri et al. 1994; Dunn and Senn 1994; see also partition coefficient data on GERM homepage under http://www-ep.es.llnl.gov/germ/Data/Partition_Coefficients

	Plagioclase	Olivine	Cpx	Opx	Ti-mag
Rb	0.08	0.005	0.005	0.005	0.005
Ta	0.04	0.005	0.008	0.01	0.01
Th	0.11	0.005	0.01	0.01	0.005
Ba	0.16	0.001	0.001	0.005	0.005
La	0.1	0.005	0.048	0.005	0.01
Ce	0.06	0.005	0.11	0.008	0.01
Nd	0.04	0.009	0.18	0.01	0.01
Sm	0.02	0.01	0.36	0.06	0.01
Eu	0.16	0.01	0.39	0.07	0.01
Tb	0.03	0.01	0.44	0.16	0.01
Yb	0.02	0.04	0.4	0.25	0.01
Lu	0.02	0.08	0.4	0.3	0.01
Hf	0.01	0.001	0.26	0.1	0.06
Zn	0.06	0.77	0.2	0.9	3.6
Sc	0.014	0.4	3.94	1.3	0.4
Co	0.03	3	1.2	2	8
Cr	0.12	1.4	10	2.6	50

the basaltic and silicic magma. The presence of discrete compositional bands, at scales of a mm and less, and of both basaltic and rhyolitic crystals in dacites, suggest limited juxtaposition times of the commingled magmas before quenching. Using the diffusivity of SiO_2 as the rate limiting control and the formulation of Blichert-Toft et al. (1992), we estimate juxtaposition times of less than months and probably hours. All banded dacite (and rhyolite) likely formed during entrainment related to eruption. In contrast, true hybrid dacites with dacite phenocrysts indicate that some mixed magma equilibrated. Minimum contact time between rhyolite and basaltic andesite was on the order of centuries to years in order to produce cm- to mm-scale hybrids, respectively.

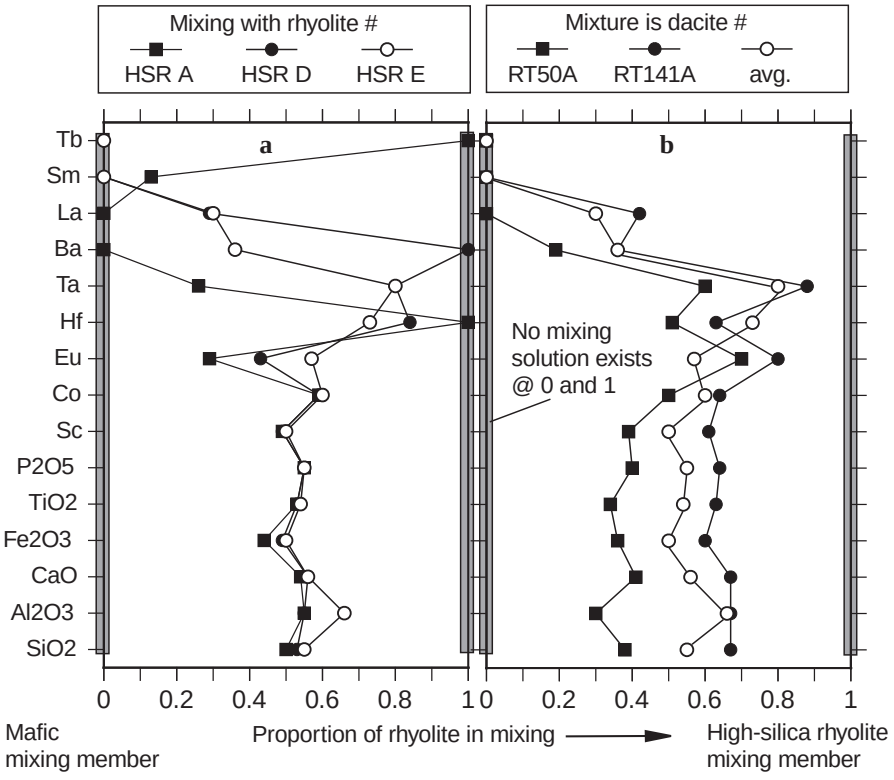

Fig. 9a, b Mixing models for dacites. Taking observed compositions for mixing endmembers (rhyolites and basaltic andesite) and mixing products (dacites), the required mixing proportion of the rhyolitic endmember was calculated for displayed elements with $\%_{\text{rhyolite in mixing}} = (C_m - C_{basalt})/(C_{rhyolite} - C_{basalt})$. C is the concentration of elements in rhyolite, basaltic andesite and mixing product (m). The mafic endmember is the average of crystal-poor inclusions for both panels **a** and **b**. **a** Rhyolite endmembers are Rattlesnake Tuff high-silica rhyolite E, D, and A (Streck and Grunder 1997) and the mixing product is average dacite (Table 1). **b** Rhyolite endmember is high-silica rhyolite E and mixing products are least silicic dacite pumice (RT50A), most silicic, least banded dacite pumice (RT141), and average dacite (*avg.*). No mixing solution exists for elements with displayed rhyolite mixing proportion of 0 and 1 (see text for interpretation)

Crossection through Rattlesnake Tuff magma chamber

The Rattlesnake Tuff magma chamber was strongly bimodal with a gap of ~20 wt% SiO_2 separating zoned high-silica rhyolites (> 280 km^3) from underlying basaltic andesite (Fig. 10). Basaltic andesite was in contact with least-evolved, high-silica rhyolite (rhyolite E), based on the presence of dacites that reflect equilibration between the two disparate compositions. The assimilation of minor rhyolite in the evolution of basaltic andesite further supports the existence of a basaltic andesite-rhyolite interface. The interface was beneath the zoned silicic part of the system, because least-evolved rhyolite, dacite, and basaltic andesite ejecta occur proximal to the vent and (or) high in the tuff (Streck and Grunder 1995).

The mafic magma occurred in distinct batches or ponds, of which some portions evolved extensively, as indicated by the diverse but related compositions of mafic inclusions and of isolated basaltic crystals. Inclusion textures range from cumulus to glomerocrystic to porphyritic and are interpreted to track different stages of solidification fronts, from nearly solid, to mush, to mainly liquid (cf., Marsh 1989). The presence of penecontemporaneous HAOT lavas, high-MgO olivines, and Cr-rich augites in some inclusions document that primitive HAOT magma was feeding into the Rattlesnake Tuff system from below.

A substantial volume of mafic magma must have underlain the silicic cap of the system, even though almost no mafic magma was erupted. Sparse but important mafic inclusions require more than 10 cycles of HAOT recharge and fractionation for every increment of basaltic andesite in order to account for their mafic

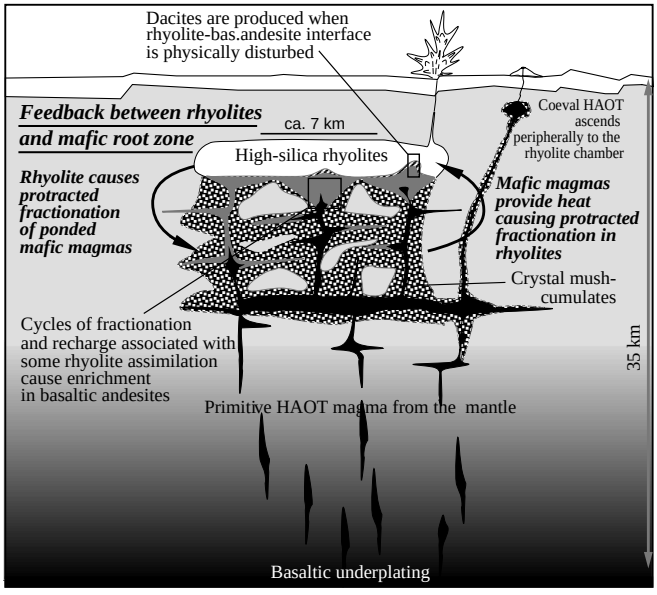

Fig. 10 Interpretative crossection through the Rattlesnake Tuff magma chamber and its mafic root zone at onset of eruption illustrating the setting for the physical and chemical feedback between the silicic and mafic parts of the system (see text)

character AND their 3–20 fold enrichment in incompatible trace elements. Even greater numbers of recharge and fractionation cycles are implied by the great incompatible element enrichments in mafic sills and inclusions in the strongly bimodal Cadillac Mountain Pluton (Wiebe 1996, 1997). Episodic recharge in the Rattlesnake Tuff system may have stimulated assimilation of rhyolite by providing heat and a physical disturbance of the mafic-silicic interface. Eruption was probably triggered by such a mafic injection event and accompanying draw-up produced the banded dacites and other commingled ejecta.

We envision a root zone of mafic magmas pooled and trapped beneath the low-density rhyolites with a volume at least as great as the rhyolitic system and likely substantially greater. Trapping and reinjection of basalt drove differentiation in the mafic zone which in turn provided the thermal feedback necessary to sustain and evolve the silicic cap.

Conclusions

Although volumetrically minor, basaltic inclusions and crystals entrained in the Rattlesnake Tuff are critical evidence for the existence of an extensive mafic root zone trapped beneath the silicic magma and for the differentiation processes within the mafic magmas. Mafic compositions range from primitive high-alumina olivine tholeiite, like that erupted regionally, to basaltic andesites with moderate to substantial enrichments in incompatible trace elements. These enrichments, together with moderate depletion of compatible trace elements and mafic bulk composition, record a history of repeated cycles of mafic injection and crystal fractionation coupled with minor contamination with rhyolite. Mafic magmas are trapped beneath rhyolite by the lesser density of the latter and thermally maintain the rhyolite at least transiently near the liquidus, allowing for extensive differentiation of the rhyolite. The intimate thermal and density feedback between the silicic and mafic part of the magma column leads to compositional differentiation in both.

Dacite pumices are also sparse, but provide windows into the chemical equilibration (hybrid dacites) and into forceful mingling (banded dacites) between basaltic andesite and rhyolite magmas that occurred before and during eruption.

Quenched mafic inclusions in silicic volcanic rocks, and perhaps those mafic enclaves that represent quenched mafic liquids in granitic plutons, may be substantially evolved from a primitive mafic magma whenever the silicic magma is sufficiently voluminous to trap mafic melts for long. Incompatible element enrichments coupled with basaltic bulk composition are not necessarily evidence of enriched mantle sources because the mafic character of underplated magma is maintained by recharge.

Acknowledgements This study was funded by the US National Science Foundation grant EAR-9220500 to Grunder, and by Chevron and GSA-Penrose grants to Streck. The OSU Radiation Center is thanked for gracious analytical support as well as Hans-Ulrich Schmincke for some microprobe analyses. The first author thanks Michael Dungan for hosting him as a post-doc at the Université de Genève during final preparation of the manuscript. We have benefited from discussions with many colleagues, including Mark Ghiorso, Roger Nielsen, and Peter Reiners, and particularly, Bob Wiebe. We thank Clark Johnson and Tom Wagner for reviews of a previous version of the manuscript.

References

Ariskin AA, Frenkel MY, Barima GS, Nielsen RL (1993) COMAGMAT: a FORTRAN program to model magma differentiation processes. Computers and Geosciences 19: 1155–1170

Bacon CR (1986) Magmatic inclusions in silicic and intermediate volcanic rocks. J Geophys Res 91: 6091–6112

Bacon CR, Druitt TH (1988) Compositional evolution of the zoned calc-alkaline magma chamber of Mount Mazama, Crater Lake, Oregon. Contrib Mineral Petrol 98: 224–256

Bailey DG, Conrey RM (1992) Common parent magma for Miocene to Holocene mafic volcanism in the northwestern United States. Geology 20: 1131–1134

Baker MB, Grove TL, Kinzler RJ, Donnelly-Nolan JM, Wandless GA (1991) Origin of compositional zonation (high-alumina basalt to basaltic andesite) in the Giant Crater lava field, Medicine Lake volcano, northern California. J Geophys Res 96: 21819–21842

Bartels KS, Kinzler RJ, Grove TL (1991) High pressure phase relations of primitive high-alumina basalts from Medicine Lake volcano, northern California. Contrib Mineral Petrol 108: 253–270

Blichert-Toft J, Lesher CE, Rosing MT (1992) Selective contamination of the Tertiary East Greenland macrodike complex. Contrib Mineral Petrol 110: 154–172

Boden DR (1989) Evidence for step-function zoning of magma and eruptive dynamics, Toquima caldera complex, Nevada. J Volcanol Geotherm Res 37: 39–57

Brophy JG, Dorais MJ, Donnelly-Nolan J, Singer BS (1996) Plagioclase zonation styles in hornblende gabbro inclusions from Little Glass Mountain, Medicine Lake volcano, California: implications for fractionation mechanisms and the formation of composition gaps. Contrib Mineral Petrol 126: 121–136

Carlson RW, Hart WK (1987) Crustal genesis on the Oregon plateau. J Geophys Res 92: 6191–6206

Carmichael ISE, Turner FJ, Verhoogen J (1974) Igneous petrology. McGraw Hill

Didier J, Barbari B (eds) (1991) Enclaves and granite petrology (Developments in Petrology 13) Elsevier, Amsterdam, pp 1–625

Donnelly-Nolan J, Champion DE, Grove TL, Baker MB, Taggart JE Jr., Bruggman PE (1991) The Giant Crater lava field: geology and geochemistry of a compositionally zoned, high-alumina basalt to basaltic andesite eruption at Medicine Lake volcano, California. J Geophys Res 96: 21843–21863

Draper DS (1991) Late Cenozoic bimodal magmatism in the northern Basin and Range Province of southeastern Oregon. J Volcanol Geotherm Res 47: 299–328

Dunn T, Senn C (1994) Mineral/matrix partition coefficients for orthopyroxene, plagioclase, and olivine in basaltic to andesitic systems: a combined analytical and experimental study. Geochim Cosmochim Acta 58: 771–733

Elburg MA (1996) Genetic significance of multiple enclave types in a peraluminous ignimbrite suite, Lachlan fold belt, Australia. J Petrol 37: 1385–1408

Feeley TC, Grunder AL (1991) Mantle contribution to the evolution of Middle Tertiary silicic magmatism during early stages of extension: the Egan Range volcanic complex, east-central Nevada. Contrib Mineral Petrol 106: 154–169

Feeley TC, Dungan MA (1996) Compositional and dynamic controls on mafic-silicic magma interactions at continental arc volcanoes: evidence from Cordón El Guadal, Tatara-San Pedro complex, Chile. J Petrol 37: 1547–1577
Freundt A, Schmincke HUS (1995) Petrogenesis of rhyolite-trachyte-basalt composite ignimbrite P1, Gran Canaria. J Geophys Res 100: 455–474
Frost TP, Mahood GA (1987) Field, chemical and physical constraints on mafic-felsic magma interaction in the Lamarck granodiorite, Sierra Nevada, California. Geol Soc Am Bull 99: 272–291
Green TH (1994) Experimental studies of trace-element partitioning applicable to igneous petrogenesis – Sedona 16 years later. Chem Geol 117: 1–36
Greene RC (1973) Petrology of the welded Tuff of Devine Canyon, southeastern Oregon. US Geol Survey Prof Pap 797
Greene RC, Walker GW, Corcoran RE (1972) Geologic map of the Burns quadrangle, Oregon. US Geol Survey map I-680
Grove TL, Donnelly-Nolan (1986) The evolution of young silicic lavas at Medicine Lake volcano, California: implications for the origin of compositional gaps in calcalkaline lava series. Contrib Mineral Petrol 92: 281–302
Grove TL, Kinzler RJ, Baker MB, Donnelly-Nolan JM, Lesher CE (1988) Assimilation of granite by basaltic magma at Burnt lava flow, Medicine Lake volcano, northern California: decoupling of heat and mass transfer. Contrib Mineral Petrol 99: 320–343
Hart SR, Dunn T (1993) Experimental cpx/melt partitioning of 24 trace elements. Contrib Mineral Petrol 113: 1–8
Hart WK, Aronson JL, Mertzman SA (1984) Areal distribution and age of low-K, high-alumina olivine tholeiite magmatism in the northwestern Great Basin. Geol Soc Am Bull 95: 186–195
Hauri EH, Wagner TP, Grove TL (1994) Experimental and natural partitioning of Th, U, Pb and other trace elements between garnet, clinopyroxene and basaltic melts. Chem Geol 117: 149–166
Hildreth W (1987) New perspective on the eruption of 1912 in the Valley of Ten Thousand Smokes, Katmai National Park, Alaska. Bull Volcanol 49: 690–693
Johnson JA (1995) Geologic evolution of the Duck Creek Butte eruptive center, High Lava Plains, southeastern Oregon. Master's thesis, Oregon State University, Corvallis
Le Bas MJ, Le Maitre RW, Streckeisen A, Zanettin B (1986) A chemical classification of volcanic rocks based on the total alkali-silica diagram. J Petrol 27: 745–750
Linneman SR, Myers JD (1990) Magmatic inclusions in the Holocene rhyolites of Newberry volcano, central Oregon. J Geophys Res 95: 17677–17691
Lofgren G (1980) Experimental studies on the dynamic crystallization of silicate melts. In: Hargraves RB (ed) Physics of magmatic processes. Princeton University Press, Princeton NJ, pp 478–551
MacLean JW (1994) Geology and geochemistry of Juniper Ridge, Horsehead Mountain and Burns Butte: implications for the petrogenesis of silicic magma on the High Lava Plains, southeastern Oregon. Master's thesis, Oregon State University, Corvallis
MacLeod NS, Walker GW, McKee EH (1976) Geothermal significance of eastward increase in age of upper Cenozoic rhyolitic domes in southeastern Oregon. Second United Symposium on the development and use of geothermal resources, Proceedings 1: 465–474
Marsh BD (1989) On convective style and vigor in sheet-like magma chambers. J Petrol 30: 479–530
McBirney AR (1996) The Skaergaard Intrusion. In: Cawthorne RG (ed) Layered Intrusions (Developments in Petrology 15). Elsevier, Amsterdam, pp 147–180
McKee EH, Duffield WA, Stern RJ (1983) Late Miocene and early Pliocene rocks and their implications for crustal structure, northeastern California and south-central Oregon. Geol Soc Am Bull 94: 292–304
Naslund HR (1989) Petrology of the Basistoppen sill, east Greenland: a calculated magma differentiation trend. J Petrol 30: 299–319
Parker DJ (1974) Petrology of selected volcanic rocks of the Harney Basin, Oregon. PhD thesis, Oregon State University, Corvallis
Peck DL, Wright TL, Moore JG (1966) Crystallization of tholeiitic basalt in Alae lava lake, Hawaii. Bull Volcanol 29: 929–56
Roeder PL, Emslie RF (1970) Olivine liquid equilibrium. Contrib Mineral Petrol 29: 275–289
Skulski T, Minarik W, Watson EB (1994) High-pressure experimental trace-element partitioning between clinopyroxene and basaltic melts. Chem Geol 117: 127–147
Sparks RSJ, Marshall LA (1986) Thermal and mechanical constraints on mixing between mafic and silicic magmas. J Volcanol Geotherm Res 29: 99–124
Streck MJ (1994) Volcanology and petrology of the Rattlesnake Tuff. PhD thesis, Oregon State University, Corvallis
Streck MJ, Grunder AL (1995) Crystallization and welding variations in a widespread ignimbrite sheet: the Rattlesnake Tuff, eastern Oregon. Bull Volcanol 57: 151–169
Streck MJ, Grunder AL (1996) Strong local trace element variability in a tholeiitic suite from Oregon: dominance of intrasuite interactions vs. mantle or crustal processes. Abstracts Goldschmidt '96 Conference, Heidelberg, p-603
Streck MJ, Grunder AL (1997) Compositional gradients and gaps in high-silica rhyolites of the Rattlesnake Tuff, Oregon. J Petrol 38: 133–163
Sutton AN, Blake S, Wilson CJN (1995) An outline geochemistry of rhyolite eruptives from Taupo volcanic centre, New Zealand. J Volcanol Geotherm Res 68: 153–175
Valentine GA (1993) Note on the distribution of basaltic volcanism associated with large silicic centers. J Volcanol Geotherm Res 56: 167–170
Walker GW (1970) Cenozoic ash-flow tuffs of Oregon. Oreg Dep Geol Miner Ind 32: 97–115
Walker GW (1974) Some implications of late Cenozoic volcanism to geothermal potential in the High Lava Plains of south-central Oregon. The Ore Bin 36: 109–123
Walker GW (1979) Revisions to the Cenozoic stratigraphy of Harney basin, southeastern Oregon. US Geol Surv Bull 1475: 1–35
Walker GW, Nolf B (1981) High lava plains, Brothers fault zone to Harney Basin, Oregon. In: Johnston DA, Donnelly-Nolan J (eds) Guides to some volcanic terranes in Washington, Idaho, Oregon, and northern California. US Geol Surv Circular 838, pp 105–112
Walter RC, Hart WK, Westgate JA (1987) Petrogenesis of a basalt-rhyolite tephra from the west-central Afar, Ethiopia. Contrib Mineral Petrol 95: 462–480
Watson EB (1976) Two liquid partition coefficients: experimental data and geochemical implications. Contrib Mineral Petrol 56: 119–134
Wiebe RA (1996) Mafic-silicic layered intrusions: the role of basaltic injections on magmatic processes and the evolution of silicic magma chambers. Trans R Soc Edinburgh 87: 233–242
Wiebe RA (1997) Enclaves in the Cadillac Mountain Granite (coastal Maine): samples of hybrid magma from the base of the chamber. J Petrol 38: 393–423
Wright TL, Fiske RS (1971) Origin of differentiated and hybrid lavas of Kilauea volcano, Hawaii. J Petrol 12: 1–65
Yang HJY, Kinzler RJ, Grove TL (1996) Experiments and models of anhydrous, basaltic olivine-plagioclase-augite saturated melts from 0.001 to 10 kbar. Contrib Mineral Petrol 124: 1–18